University of Alberta

Radio Frequency Characterization and Modelling of Low Temperature Co-Fired Ceramic (LTCC) Material and Devices

by

Fatemeh Kalantari

A thesis submitted to the Faculty of Graduate Studies and Research
in partial fulfillment of the requirements for the degree of

Master of Science

in

Integrated Circuits and Systems

Department of Electrical and Computer Engineering

Spring 2014
Edmonton, Alberta

To my beloved family.

Abstract

The focus of this dissertation is on the characterization of Low Temperature Co-fired Ceramic (LTCC) for microwave and Radio Frequency (RF) applications. The LTCC substrates' excellent microwave properties make them great candidates for the packaging of RF devices, as well as the fabrication of passive RF and microwave components. In order to utilize LTCC, the first step is to characterize its microwave properties including the dielectric constant and loss tangent which will enable designers to design and simulate the RF behavior of LTCC components accurately. Investigating various measurement techniques, we decided to use a parallel plate capacitor for the characterization of a LTCC substrate from 100 MHz to 1 GHz and a conductor backed coplanar waveguide from 1 GHz to 10 GHz. After fabrication of several test structures on Dupont 951 LTCC substrates, the scattering parameters were measured using a 110 GHz Vector Network Analyzer and the effect of the pads were de-embedded from measurement results. Through this process, we developed a novel fast de-embedding method which de-embeds the effect of the pads and parts of the transmission lines as opposed to the conventional method, where only the effect of the pads is removed. This will result in a similar electromagnetic field around the de-embedded structure to that of a test structure where no pad exists. Therefore, the proposed de-embedding method produces more accurate loss tangent and dielectric constant results compared to the conventional method.

Acknowledgements

I owe my profound gratitude to my supervisor Dr. Kambiz Moez whose encouragement, support and valuable advice has led me to go through this program and to make this work a success. It has been a great privilege to be a part of his research team.

I would like to express my grateful thanks to Mr. Kevin Yallup, CTO of Alberta Centre for Advanced MNT Products (ACAMP), our project partner, for defining this project and the engaging assistance from the University of Alberta and providing us with their Dupont 951 LTCC products.

I am grateful to my colleagues and lab mates in Electrical and Computer program for their help and support in various aspects of my research.

Finally, I would like to express my appreciation to my husband and my family for their caring and supportive attitude in all aspects of my life.

Contents

List of Tables

List of Figures

List of Symbols

W: Width of signal conductor in a transmission line.

S: Spacing between conductor and ground planes.

H: Thickness of substrate.

t: Thickness of signal conductor.

ε_r: Relative dielectric constant.

ε: Dielectric constant.

Z_0: Characteristic impedance.

ε_{eff}: Effective dielectric constant.

K (k): complete elliptic integral of the first kind

S_{11}: Input reflection coefficient of DUT.

S_{21}: Forward transmisssion coefficient of DUT.

S_{22}: Output reflection coefficient of DUT.

S_{12}: Reverse transmission coefficient of DUT.

κ: Dielectric constant of the material.

ε_0: 8.85 x 10-12 *F/m* is the free space permittivity.

A: Area of the plates.

d: Plate separation.

σ: 6.3*e+07 S/m is the electrical conductivity.

L: transmission line length.

α: Attenuation constant in decibel per centimeter.

β: the phase constant in *cm-1*.

$\Delta\Phi S_2$: the phase shift of transmission coefficient S_{21}.

R: Resistance.

L: Inductance.

C: Capacitance.

G: Conductance.

$tan\delta$: Loss tangent.

Acronyms

LTCC Low Temperature Co fired Ceramic

HTCC High Temperature Co fired Ceramic

CBCPW Conductor-Backed Coplanar Waveguides

CPW Coplanar Waveguides

VNA Voltage Network Analyzer

DUT Device Under Test

MUT Material Under Test

ACAMP Alberta Centre for Advanced MNT Products

RF Radio Frequency

RFIC Radio Frequency Integrated Circuits

CAD Computer Aided Device

ADS Advanced Design System

EM Electro-Magnetic

MEMS Micro Electromechanical Systems

MMIC Monolithic Microwave Integrated Circuits

MIC Microwave Integrated Circuits

GSG Ground Signal Ground

MATLAB Matrix Laboratory

Chapter 1

Introduction

1.1 Motivation

The continuing growth in wireless communication demands the development of low-cost RF/microwave components, which are required for the operation of wireless systems [1]. While semiconductor technologies such as Complementary Metal Oxide Semiconductor (CMOS) are extensively used for integrating all of the components of wireless transceivers onto a single chip, the packaging of these integrated circuits and their connections to off-chip components remains a challenge when developing fully integrated wireless systems [2, 3]. As a result, there is strong demand for the development of packaging technologies that offer excellent microwave properties and great compatibilities with advanced semiconductor processes.

While the majority of wireless devices and systems use conventional printed circuit boards, it is becoming obvious that this kind of technology does not cover the microwave and RF performance needs of a circuit for the commercial or technical field [4]. Recently, Low Temperature Co-fired Ceramic (LTCC), which was originally developed for the application in high temperature electronic packaging, has been considered as an excellent candidate for RF/microwave

applications [5]. LTCC technology is a multi-layer ceramic with an excellent combination of properties for high frequency applications where stable and uniform properties are required over a wide frequency range. LTCC's three dimensional structures that have buried, native passive components offers a higher circuit density than organic laminate technologies [6].The new gold and silver conductor system, DuPont Green Tape™ LTCC material, was developed for high frequency applications up to 100GHz where low loss characteristics are desired [5,6].

Green (Unfired) Dupont tape is provided in different sheet sizes and thicknesses, it is cast on polyester backing suitable for processing along with the individual layers. The process flow consists of preconditioning in a nitrogen dry box for 24 hours. Then, in each tape layer, vias for the electrical connections are formed using mechanical punching or laser drilling. Next, the conductors are created using a traditional thick film screen printer [7]. Co-firing and post-firing processes are the procedures which would be applied to the resistors, dielectrics and conductors. At the end of the fabrication process, the final inspection is done on all of the laminate samples according to an applicable standard; a detailed process flow of Dupont 951 is described in [8, 9].

Accurate designing at radio frequencies requires precise knowledge of the substrate material's characteristics such as the dielectric constant and loss tangent, to enable circuit designers to predict the RF/microwave properties of the LTCC packages and components [10].

There has been a variety of measurement techniques to characterize the dielectric properties of a material based on different factors such as: the frequency range, the material properties, the temperature and the cost. For instance, using a coaxial probe is best for lossy Material under Test (MUT) that are liquid or semi-solids since it is a broadband, convenient, non-destructive method. While for high temperature, large flat samples, it is more convenient to apply a non-contacting free space measurement to find the permittivity and permeability of the material. For small, low loss MUT samples, using a resonant cavity would fit best, and for an accurate measurement at low frequency of thin flat sheets, using a parallel plate capacitor is suggested [11, 12].

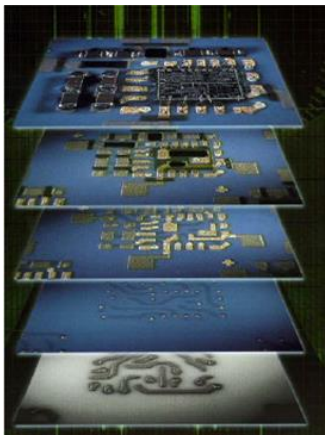

Figure 1.1. Four layer LTCC substrate with integrated passives, buried capacitors, inductors and resistors, from Dupont the miracles of science [8].

1.2 Outline of Thesis

Chapter 2 of this dissertation will briefly review the theoretical background required throughout the thesis. Physical and electrical properties of the Dupont 951 tape material that is provided by our project partner, ACAMP, will be

presented, in addition to the design parameters, and the passive and active devices' design rules. The various measurement techniques required for substrate characterization will be discussed to figure out a specific practical technique to find the dielectric constant and loss tangent of the Dupont 951 LTCC material from 100MHz to 10 GHz. Some important configurations of the transmission lines such as the Conductor- Backed Co Planar Waveguide (CBCPW), microstrip and striplines will be discussed, and their applications briefly introduced. A brief overview of the scattering parameters and a measurement technique using the Agilent vector network analyzer will be presented.

Chapter 3 reviews the dielectric characterization methods. Based on this investigation, we will conclude that the best technique to characterize the LTCC for the low frequency range is to design parallel plate capacitors, because of the parallel-plate capacitors' low resonance frequency. For the characterization of the LTCC at higher frequencies, we choose CBCPWs for their unique characteristics at high frequencies. Using Agilent App-CAD and ADS software, we design a set of CBCPWs with different dimensions. In order to verify the models, we utilize the ADS EM simulations to ensure the proper operation of the test structures in the required frequency range. The next step will be calculating the dielectric constant and loss tangent based on the "Conformal Mapping Technique" in which the measured scattering parameters are used to estimate the dielectric constant of the material. After the models are fabricated on Dupont 951 substrate, a 110 GHz VNA with its 50 ohm probe station will be used to measure the scattering parameters of the fabricated test structures. To obtain the scattering parameters of

the CBCPW test structures, the effects of the pads are de-embedded from the measured scattering parameters using a conventional de-embedding method. Finally, the dielectric constant is calculated using the "Conformal Mapping Technique".

In Chapter 4, we will propose an accurate analytical method for de-embedding the transmission lines which will result in a more accurate estimation of the dielectric properties of the material. In this method, instead of only de-embedding the pads, we de-embed the pads and parts of the connecting transmision lines to obtain an electromagnetic enviroment similar to that of a test structure without pads. As a result, the proposed method produces more accurate results compared to the conventional de-emebdding method.

Finally, the thesis will be concluded in Chapter 5 by summarizing the contributions of this work.

Chapter 2

Background

In this chapter, we will first have a brief description of the materials' dielectric constant and loss tangent. Then there will be a description of the various measurement techniques to characterize the dielectric properties of the LTCC material. Once that is established, the Dupont 951 tape material's physical and electrical properties provided by ACAMP will be presented in addition to the design parameters, and the passive and active devices' design rules. Some important transmission line structures such as the CBCPWs, microstrips and striplines will be discussed as well as a brief introduction to their applications in sections 2.4.1 through 2.4.3. Finally, we will briefly review the measuring of the scattering parameters using vector network analyzers in section 2.5.

2.1 Dielectric Constant and Loss Tangent

The dielectric constant (ε_r) is the ratio of the permittivity of a substance ($\varepsilon_{material}$) to the permittivity of free space (ε_0). It defines the extent to which a material concentrates electric flux, in other words, it is the electrical equivalent of relative magnetic permeability,

$$\varepsilon_r = \frac{\varepsilon_{material}}{\varepsilon_0}. \qquad (2.1)$$

The dielectric constant and the effective dielectric constant are two different variables. The dielectric constant is a bulk material property; the effective dielectric constant is a parameter that depends on the transmission line geometry.

Permittivity is actually a complex number that is an "epsilon" which is made up of two parts,

$$\varepsilon = \varepsilon' - j\varepsilon^{"}. \qquad (2.2)$$

Microwave engineers usually deal with the ratio between the two, which is called the tangent delta,

$$tan\delta = \frac{\varepsilon^{"}}{\varepsilon'}. \qquad (2.3)$$

If the tangent delta is zero, there is no loss due to the dielectric; for example, dry air has no dielectric loss.

In fact, the loss tangent is a parameter of a dielectric which quantifies its inherent dissipation of electromagnetic energy and is proportional to the frequency. The term refers to the tangent of the angle in a complex plane between the resistive component of an electromagnetic field and its reactive component [13].

2.2 Substrate Material Measurement Techniques

There has been a variety of measurement techniques developed to characterize a substrate material based on different factors such as: frequency range, material properties, temperature, cost and some other factors which will be described in this section [14].

2.2.1 Coaxial Probe

By immersing the open ended coaxial probe into a liquid, the material's properties are measured. If the material is solid or a powder, the probe touches it to a flat face.

The electromagnetic field at the probe end fringes into the material and changes as it makes contact with the MUT, then the forward transmission coefficient, S_{11}, is measured and the dielectric constant is calculated. In this method, the measuring system includes an impedance analyzer and software [15].

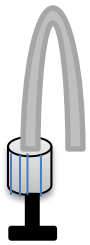

Figure 2.1. Coaxial probe method to characterize a substrate.

To specify the features of this method, we can mention its suitability for broadband application, and simplicity. It is a good measurement method for liquid and semi-solid materials with semi-infinite thickness that are non-magnetic and isotropic. In this technique we have a limited dielectric constant and a loss tangent with limited accuracy and resolution [15].

2.2.2 Transmission line

In this method, the material is placed inside a portion of an enclosed transmission line which is a rectangular waveguide or coaxial line as shown in Figure 2.2. Using vector network analyzer software such as 85071E and an external computer, the measured reflected and transmitted signals are converted to material properties including the dielectric constant and loss tangent [16].
The coaxial transmission line is difficult to manufacture but covers a wide range of frequencies, while a rectangular wave guide is simpler to machine but their frequency coverage is banded.

Figure 2.2. Transmission line method; waveguide and coaxial line case.

The features for a material under testing are: having no air gaps at the fixture walls, being smooth, having flat faces, being perpendicular to the long axis, and being homogeneous. This is a broad band method in which the low frequency is limited by the practical sample length, and depending on the sample length its low

loss resolution is limited. This method is capable of measuring magnetic and anisotropic materials [17].

2.2.3 Free Space

This method takes advantage of using some antennas to focus the microwave energy through a material without a need for a test fixture as shown in Figure 2.3. This method is applicable to high temperature materials in hostile environments, since it is a non-contacting method. The measuring system includes a vector network analyzer software such as 85071 and a computer.

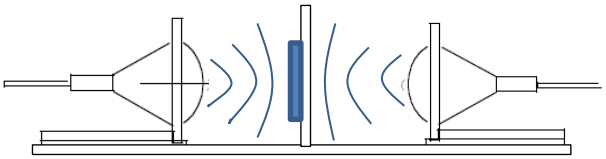

Figure 2.3. Free space measurement method.

Material assumptions are: large, flat, homogeneous, and parallel-faced samples. This method is a non-contacting non-destructive one for high temperature samples which can measure magnetic materials as well. It is a high frequency method with a low end limited by the practical sample size, in which the antenna polarization may vary with anisotropic materials [18].

2.2.4 Resonant Cavity

This is a resonant technique versus the broadband techniques talked about previously. Resonant cavities are structures with high quality factors that resonate at certain frequencies, in which a piece of sample material affects their quality factor and centre frequency. The complex permitivity, ε_r , is then calculated from

these parameters at a single frequency using a network analyzer software and an external computer. The most widely purterbation cavity method as described in [19] uses a rectangular wave guide with iris-coupled end plates which operates in the TE_{10n} mode, as shown in Figure 2.4. To measure the dielectric constant, the sample is inserted in the middle of a wave guide length, then an odd number of half wavelengths will cause a maximum electric field which can lead to a dielectric constant measurement.

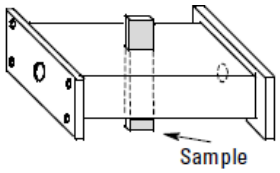

Figure 2.4. Resonant cavity measurement method.

Resonant techniques are practical in high impedance environments, but only at one or a few frequencies. These measurements are well suited for small samples and low loss materials. While broad band techniques require low impedance environments and the measurement can be done at any frequency, they need larger samples to obtain reasonable measurements.

2.2.5 Parallel Plate Capacitor

In this method, a thin sheet of material is inserted between two electrodes to form a capacitor. The measuring system consists of an impedance analyzer and a fixture. More information on the low frequency materials' measurement solutions is available in the application notes [20, 21].

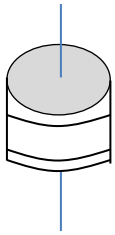

Figure 2.5. Parallel plate measurement method.

2.2.6 Comparison of Characterization Methods

Many factors are important in selecting the most appropriate measurement technique such as: the frequency range, the required measurement accuracy, the material properties and form, the sample size restrictions, whether it needs to be destructive or non-destructive, contacting or non-contacting, the temperature and the cost. Since our concern is to work in a wide frequency range, the resonant cavity methods would be useless because resonant techniques are practical at one or a few frequencies. The free space measuement technique is applicable to high temperature materials in hostile environments, but we have our measurements at room temperature. Coaxial probe technique is a good measurement method for liquid and semi-solid materials with semi-infinite thickness; however our concern is to measure the dielectric properties of a solid and very thin substrate. Other than that, coaxial probe method offers a limited dielectric constant and a loss tangent with limited accuracy and resolution. Thus taking advantage of the transmission line method would be the best decision since the features for a material under test mentioned in Section 2.2.2 is completely compatible to Dupont 951 substrate. In this method, the material is placed inside a portion of enclosed CBCPWs which are accurately measurable using our in-house vector

network analyzer. Besides, the transmission line method is a broad band technique and would be appropriate for our frequency range of 1GHz to 10 GHz. However, for frequencies from 100 MHz to 1 GHz using the parallel plate capacitor seems to be more appropriate since this is a simple, accurate method for low frequencies and works properly for thin, flat sheet samples such as our six layer 600 µm LTCC.

2.3 ACAMP Design Parameters

Dupont 951 tape material's physical and electrical properties are provided in Table 2.1.

Table 2.1. Dupont 951 tape material physical and electrical properties [22].

Dupont 951 Tape	**Physical and electrical properties**
Substrate thickness	50,114,165,254
Substrate size	150 mm * 150 mm
Dielectric constant	7.8 at 1MHz
Insulation resistance	1*10^12 ohm
Fired effective area	130 mm * 130 mm
X-Y shrinkage	12.7% +/- 0.3%
Z shrinkage	15.0% +/- 0.5%
Density	3.1 g/cm^3
Dissipation factor	0.15%
Breakdown voltage	>40,000 volts/mm

Table 2.2 shows Dupont 951 tape material's thermal and mechanical properties [22].

Table 2.2. Dupont 951 tape material thermal and mechanical properties [22].

Dupont 951 Tape	**Thermal and mechanical Properties**
Conductivity	3.0 W/m.k
Young's modulus	152 GPa
Fracture strength	320 MPa
Expansion coefficient	5.8 ppm/C
Specific heat	0.989 J/gC
Surface roughness	<10 Micro-inches

Dupont 951 tape's design parameters are shown in Table 2.3.

Table 2.3. Dupont 951 tape design parameters and considerations [23].

Conductors	**Preferred**	**Advanced**	**Minimum**
Line width	150 um	30 um	100 um
Line to line spacing	150 um	30 um	100 um
Line to via pad spacing	150 um	30 um	100 um
Line to part edge spacing	500 um	250 um	250 um
Internal conductors	Silver, Gold	Silver, Gold	Silver, Gold
External conductors	Silver-Palladium, Gold	Silver-Palladium, Gold	Silver-Palladium, Gold
VIAS			
Diameter	250 um	100 um	150 um
Thermal via	250 um	250 um	250 um

Table 2.4 presents Dupont 951 tape's considerations for passive devices [23].

Table 2.4. Dupont 951 tape design parameters and considerations for passive devices.

Capacitors	
Dielectric thickness	>16 um
Area	<150 mm^2
Dielectric paste	K=250, 500
Internal conductors	Silver, Gold
External conductors	Silver-Palladium, Gold
Precision	5-10%
Inductors	
Conductors	As per conductor spec.
Vias	As per via spec.
Resistors	
Length	750 um min.
Width	750 um min.
Resistance	Tunable by aspect ratio
Sheet resistance	10, 100, 1000, 10000
Precision as fired	35%
Material	Ruthenium oxide
Overlap	250 um min.

Several passive RF/microwave components can be constructed using a LTCC process. A sample Spiral inductor with gold on Tape 951 from Dupont is shown in Figure 2.6, and in Figure 2.7, we can see a dual port and single port, multi finger and single capacitors with gold on Tape 951 from Dupont [24, 25].

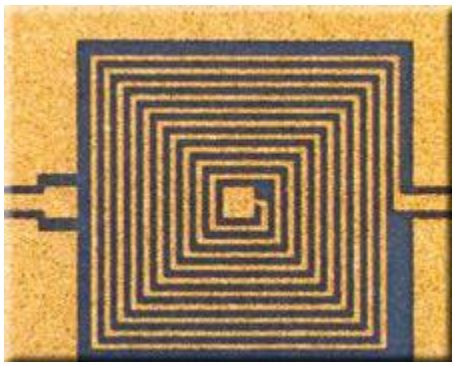

Figure 2.6. Spiral inductor with gold on Tape 951 from Dupont [24].

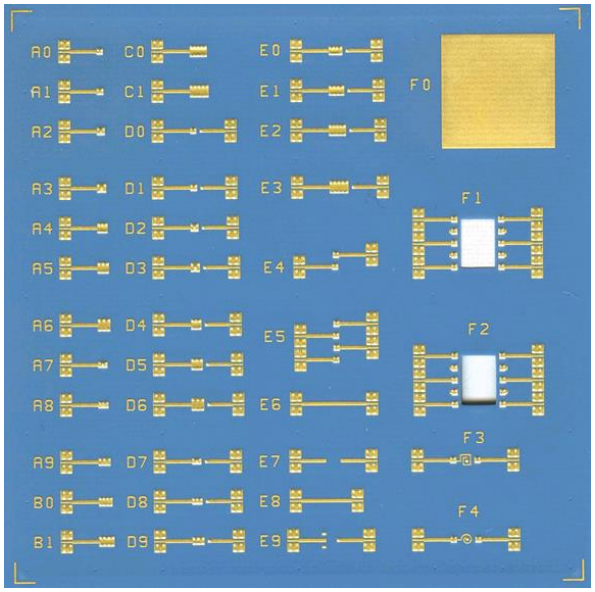

Figure 2.7. Dual port and single port, multi finger and single capacitors with gold on Tape 951 from Dupont [25].

Figure 2.8 shows a sample of fabricated resistors on Tape 951 from Dupont [26].

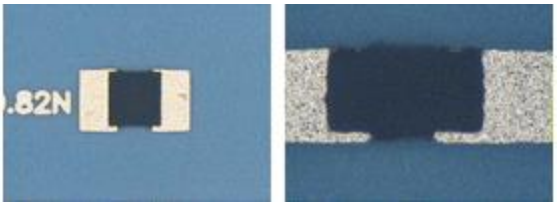

Figure 2.8. Resistors on Tape 951 from Dupont [26].

DuPont offers two various tape compositions: 951 Green Tape and 943 Green Tape. 951 Green Tape consists of high strength glass or a ceramic composite which is suitable for applications below 20 GHz, and 943 Green Tape is a lead-free glass ceramic composition and designed for applications up to 100 GHz. We have applied 951 Green Tape systems of materials considering our frequency range [22].

Ag and Au co-fired metallization are available for 951 Green tape systems, in practice they use the combination of Ag for internal conductors and Au for external conductors and wire bonding. In order to cut the cost, we applied Ag as our conductors [27].

2.4 Transmission lines

Specific transmission line structures including coplanar wave guides, striplines and microstrips have been considered greatly for characterizing materials [28, 29].

2.4.1 CBCPW

There are two main structures of coplanar lines, Coplanar Wave guides (CPW) with no lower ground plane as illustrated in Figure 2.9 and Conductor-Backed Coplanar Wave guides (CBCPW) with a lower ground plane known as CBCPW as illustrated in Figure 2.10, [30,31].

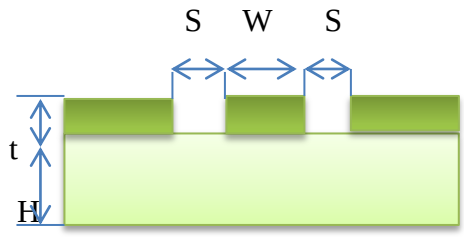

Figure 2.9. Coplanar Waveguides (CPW) with no lower ground plane.

W is the conductor width, *S* denotes the space between conductor and the ground planes while *H* represents dielectric thickness and *t* is the conductor thickness.

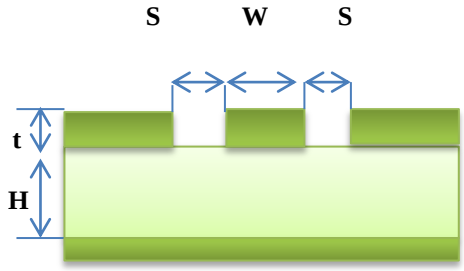

Figure 2.10. Conductor-Backed Coplanar Waveguides (CBCPW) with lower ground plane.

A common approach to having an optimized CBCPWdesign is to consider the limitations as

$$\begin{aligned} &H>b \\ &W>b \\ &S=2a \\ &b=W+2S=246+2*100=446\ um \\ &H=100*6=600\ um. \end{aligned} \tag{2.4}$$

To accurately predict the conductor-backed coplanar wave guides' characteristic impedance, we need to calculate the effective dielectric constant as

$$Z_0 = \frac{30\pi}{\sqrt{\varepsilon_{eff,t}}} . \frac{K(k_t')}{K(k_t)}. \qquad (2.5)$$

ε_{eff} is the effective dielectric constant and *K* is the complete elliptic integral of the first kind which can be calculated using MATLAB software as

$$\varepsilon_{eff,t} = \varepsilon_{eff} - \frac{\varepsilon_{eff} - 1.0}{\frac{\frac{b-a}{2.0}}{0.7t} . \frac{K(k_t')}{K(k_t)} + 1.0} . \quad (2.6)$$

where *a* is half of the spacing between the conductor and the ground planes and *b* is *W+2S* as shown in (2.4), and we have

$$\varepsilon_{eff} = 1 + \frac{\varepsilon_r - 1.0}{2.0} . \frac{K(k')}{K(k)} . \frac{K(k1)}{K(k'1)}, \qquad (2.7)$$

where ε_r is the relative dielectric constant of the substrate and *K(k)* is the complete elliptic integral of the first kind which can be calculated using MATLAB as

$$k_1 = \frac{sinh(\frac{\pi a_t}{4.0h})}{sinh(\frac{\pi b_t}{4.0h})}$$

$$k'1 = \sqrt{1.0 - k1^2}$$

$$k_t = \frac{a_t}{b_t}$$

$$k_t' = \sqrt{1.0 - {k_t}^2}$$

$$k = \frac{a}{b}$$

$$k' = \sqrt{1.0 - k^2},$$

where

$$a_t = a + \frac{1.25t}{\pi}\left[1.0 + ln\left(\frac{4.0\pi a}{t}\right)\right]$$

$$b_t = b - \frac{1.25t}{\pi}\left[1.0 + ln\left(\frac{4.0\pi a}{t}\right)\right].$$

2.4.2 Stripline

The stripline calculations would be more specific when taking into consideration the parallel plate assumptions and the large ground plane with zero thickness. To accurately predict the stripline impedance, we must calculate the effective dielectric constant [32].

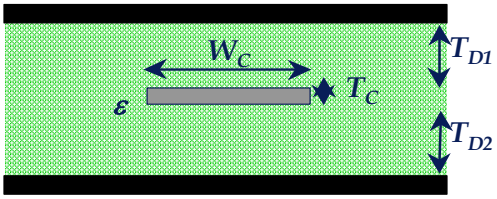

Figure 2.11. Symmetric (balanced) stripline, case $T_{D1} = T_{D2}$.

T_C is the conductor's thickness and W_C represents the conductor's width and ε is the dielectric constant of the substrate. For the Symmetric (balanced) stripline case, $T_{D1} = T_{D2}$ the characteristic impedance of the system, Z_{0sym} will be

$$Z_{0sym} \approx \frac{60}{\sqrt{\varepsilon_r}} \ln\left(\frac{4(T_{D1}+T_{D1})}{0.67\pi(0.8W_C+T_C)}\right), \tag{2.8}$$

where ε_r is the relative dielectric constant, this equation is valid when

$$W_C/(T_{D1}+T_{D2}) < 0.35 \text{ and } T_C/(T_{D1}+T_{D2}) < 0.25.$$

For the offset (unbalanced) stripline Case, $T_{D1} > T_{D2}$ we have

$$Z_{0offset} \approx 2\frac{Z_{0sym}(2A,W_C,T_C,\varepsilon_r)\cdot Z_{0sym}(2B,W_C,T_C,\varepsilon_r)}{Z_{0sym}(2A,W_C,T_C,\varepsilon_r)+Z_{0sym}(2B,W_C,T_C,\varepsilon_r)}, \tag{2.9}$$

where $T_{D1}= 2A$ and $T_{D2}= 2B$, [32].

2.4.3 Microstrip

The microstrip line calculations would be more specific when the parallel plate assumptions and the large ground plane with zero thickness are taken into consideration. To accurately predict the microstrip line impedance, we must calculate the effective dielectric constant [33].

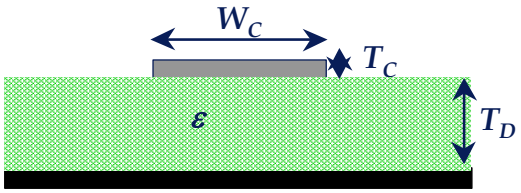

Figure 2.12. Microstrip transmission line.

T_C is the conductor's thickness and W_C represents conductor's width and ε is the dielectric constant of the substrate.

The characteristic impedance would be

$$Z_0 \approx \frac{87}{\sqrt{\varepsilon_r + 1.41}} \ln\left(\frac{5.98T_D}{0.8W_C + T_C}\right). \tag{2.10}$$

This formula is valid when

$$0.1 < W_C/T_D < 2.0 \text{ and } 1 < \varepsilon_r < 15$$

where

$$\varepsilon_e = \frac{\varepsilon_r + 1}{2} + \frac{\varepsilon_r - 1}{2\sqrt{1 + \frac{12T_D}{W_C}}} + F - 0.217(\varepsilon_r - 1)\frac{T_C}{\sqrt{W_C T_D}},$$

and F is

$$F = \begin{cases} 0.02(\varepsilon_r - 1).\left(1 - \frac{W_C}{T_D}\right) & for \ \frac{W_C}{T_D} < 1. \\ 0 & for \ \frac{W_C}{T_D} > 1 \end{cases}$$

The first requirement to design a transmission line is to choose specific line lengths in order to prevent the network analyzer from becoming ill-conditioned [34].

Mr. Hoer defines two conditions for this purpose: first, the electrical length must not be too near multiples of 180 and second, the physical length of a line whose electrical length is less than 180° may be too short to be practical.

2.5 Measurement

2.5.1 Scattering Parameters

The scattering parameters describe the electrical behavior of linear electrical networks when they are stimulated by electrical signals. Figure 2.13 shows a device under the test's transmitted, incident and reflected signals [35].

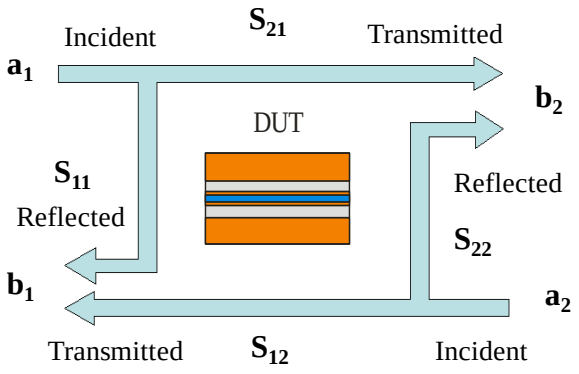

Figure 2.13. DUT transmitted, incident and reflected signals.

If the output is terminated to a perfect Z_0 load, by measuring the magnitude and the phase of incident, reflected and transmitted signals we can determine S_{11} and

S_{21}. This condition is equivalent to $a_2=0$. S_{11} represents the input reflection coefficient or the impedance of the DUT, while S_{21} is the forward transmisssion coefficient [36].

If port 1 is terminated with a perfect load and we place the source at port 2 which makes $a_1=0$, S_{22} then S_{12} can be measured. S_{22} is the output reflection coefficient or the output impedance of DUT and S_{12} is the reverse transmission coefficient as in

$$\begin{aligned} S_{11} &= \left.\frac{b_1}{a_1}\right|_{a_{2=0}} \\ S_{21} &= \left.\frac{b_2}{a_1}\right|_{a_{2=0}} \\ S_{22} &= \left.\frac{b_2}{a_2}\right|_{a_{1=0}} \\ S_{12} &= \left.\frac{b_1}{a_2}\right|_{a_{1=0}} . \end{aligned} \qquad (2.11)$$

2.5.2 The Vector Network Analyzer (VNA)

At high frequencies it is difficult to measure voltages and currents. On the other hand, at high frequencies it is easy to measure the reflection and transmission of electrical networks using network analyzers to measure the S–parameters [37].

A VNA combined with Cascade Microtech's 50-ohm probes provides a powerful tool for IC characterization, verification and measurement [38].

In order to make relevant measurements, the Network Analyzer has to be calibrated for the desired range of frequency each time. The calibration process

means determining the systematic sources of errors which is implemented by measuring known standards. Calibration removes mathematical errors from subsequent measurements and shifts the reference planes of the measurements [39].

Chapter 3

LTCC Dielectric Characterization

This chapter begins with a description of the selected test structures for LTCC characterization at low and high frequencies. The parameters of the parallel plate capacitors, CBCPWs, microstrips and striplines are discussed in details. The calculations of the dielectric constant and loss tangent based on the Conformal Mapping Technique will be discussed in Section 3.4. The next section will introduce the test setup, which uses a 110 GHz VNA and a probe station for the S-parameters measurements. In Section 3.5, the measurement data and ADS simulated results will be compared. The de-embedding process of ports will be described in Section 3.6 and the calculated dielectric constant and loss tangent will be presented. Chapter 3 will conclude with a summarization in Section 3.7.

3.1 Introduction

For a low frequency range of 100 MHz to 1 GHz, the best technique to characterize the LTCC would be using a parallel plate capacitor as described previously in Chapter 2.2.6.

When designing these parallel plate capacitors, we need to consider the Dupont 951 LTCC design rules and parameters. For the characterization of the LTCC in a higher frequency range of 1 GHz to 10 GHz, it requires employing Conductor-Backed Coplanar Waveguides (CBCPW) with a lower ground plane, as described previously in Chapter 2.2.6. CBCPWs have unique characteristics and performance at high frequencies such as ready access to the ground plane, lower dispersion, and less radiation loss compared to microstrips and striplines. In addition, these types of transmission lines offer mechanical stability, thermal dissipation capability, ease of fabrication and integration capability that are attributed to the lower ground metallization. Using Agilent App CAD software, we designed a set of different types of transmission lines with their LTCC design rules in mind. To evaluate the expected measurement results, the designed structures are simulated using an Agilent Design Systems (ADS) momentum electromagnetic simulator. After fabricating the designed test structure, the scattering parameters of our designed structures are measured using our in-house VNA through a 50 ohm probe station. The next step would be calculating the dielectric constant and loss tangent based on the "Conformal Mapping Technique" using the measured scattering parameters.

3.2 Low Frequency Characterization (100 MHz to 1 GHz)

The capacitance can be easily calculated if the geometry of the conductors and the dielectric properties of the insulator between the conductors are known [40]. For

example, the capacitance of a parallel-plate capacitor made of two parallel plates, both with an area of *A* separated by a distance *d* is approximately equal to

$$C = \frac{k\varepsilon_0 A}{d}, \qquad (3.1)$$

where "κ" is the is the dielectric constant of the material, $\varepsilon_0 \approx 8.85$ x 10-12 *F/m* which is the free space permittivity, and *C* is the capacitance. Knowing the dimensions of a parallel plate capacitor, the dielectric constant of the insulator material can be easily calculated as a function of its measured capacitance using

$$k = \frac{Cd}{\varepsilon_0 A}. \qquad (3.2)$$

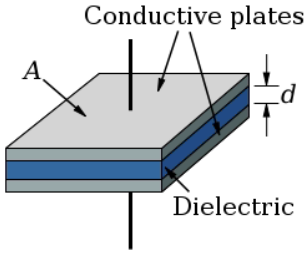

Figure 3.1. Ideal parallel plate capacitor, *A* is the area of the plates, and *d* is the plate separation.

We have designed five parallel plate capacitors for a frequency range of 100 MHz to 1GHz, according to the design rules summarized in Table 3.1, [41].

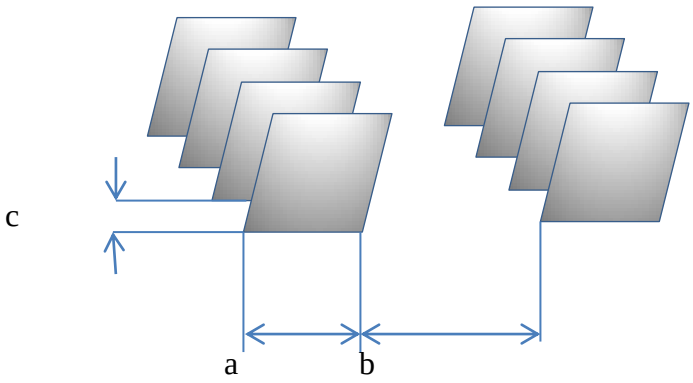

Table 3.1. Design Guidelines for LTCC according to Hirai [41].

Item	Std.
a Capacitor Size [mm]	**~5.0**
b Spacing [mm]	**>a**
c Distance among each layers [um]	**~40**

Using Agilent Advanced Design System software, we obtained the scattering parameters of our capacitors, assuming "κ" of 7.99 for the preliminary simulation of the LTCC parallel-plate capacitors. The simulated scattering parameters that are used to predict the measurement data base after de-embedding will eventually be used to determine the dielectric constant and loss tangent of the LTCC substrate from 100MHz to 1 GHz.

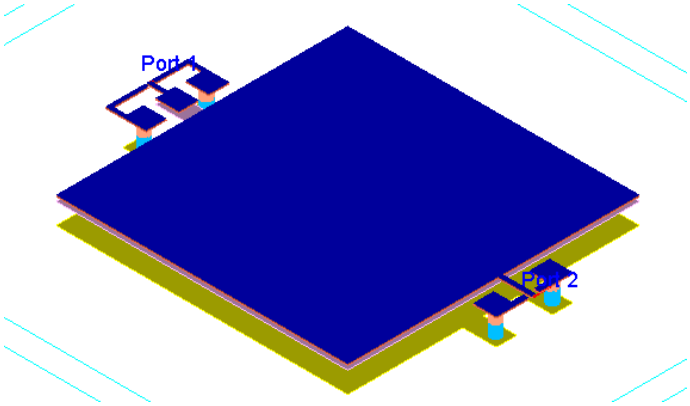

Figure 3.2. Three dimensional visualization of our designed capacitors in Agilent Advanced Design System.

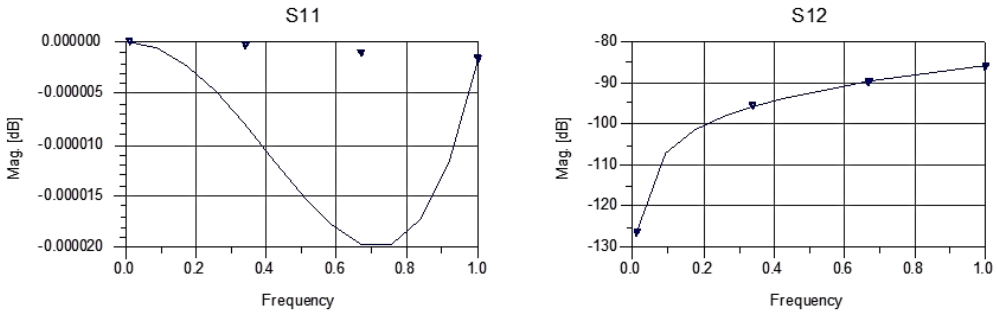

Figure 3.3. Scattering parameters of a capacitor with *A*=7*7 mm^2, and *d*=100 um, "κ" =7.99, *T*=6 um, σ=6.3*e+07 S/m.

3.3 High Frequency Characterization (1GHz to 10 GHz)

Conductor-Backed Coplanar Waveguides (CBCPW) with lower ground planes are widely used in Microwave Integrated Circuits (MICs) and Monolithic Microwave Integrated Circuits (MMICs). CBCPWs have demonstrated to be the most appropriate candidates for LTCC characterization due to their characteristics and performance at higher frequencies. In addition to having ready access to the ground plane, mechanical stability, thermal dissipation capability, and ease of fabrication and integration capability, CBCPWs offer lower dispersion and less

radiation loss compared to microstrip lines and striplines. Taking into account some dimensional restrictions, several coplanar transmission lines with different dimensions were designed as listed in Table 3.3. As can be seen in Figure 3.4, fourteen sets of coplanar wave guides, ten micro striplines and twelve sandwich striplines were designed; they were simulated using the Agilent Design Systems Momentum Electromagnetic Simulator and are listed in Table 3.2 for comparison. For preliminary simulations, a dielectric constant value of 7.99 was assumed for the LTCC substrate. Silver was used as the conductor with an electrical conductivity value of 6.3*10^7 S/m, while the conductor's thickness, *T*, is 6 µm. The width of the conductor, *W*, is designed such that the transmission line is matched to 50 ohm. We used six layers of LTCC substrates each with 100 um width, which gives the height of the substrate as *H=6*100=600* um.

L is the length of our test structures which is a multiple of λ/4.

Table 3.2. Design parameters of the CPWs, microstrips and striplines.

CPW					Microstrip				Stripline			
L mm	S µm	T µm	H µm	W µm	L mm	T µm	H µm	W µm	L mm	T µm	H µm	W µm
1.150	100	6	600	258	2.65	12	600	761	2.65	6	600	151
2.65	100	6	600	258	3	12	600	761	2.65	6	600	151
5.150	100	6	600	258	7.115	12	600	761	3	6	600	151
10.150	100	6	600	258	26.5	12	600	761	7.115	6	600	151
26.5	100	6	600	258	71.15	12	600	761	26.5	6	600	151
81.6	100	6	600	258	95	12	600	761	95	6	600	151

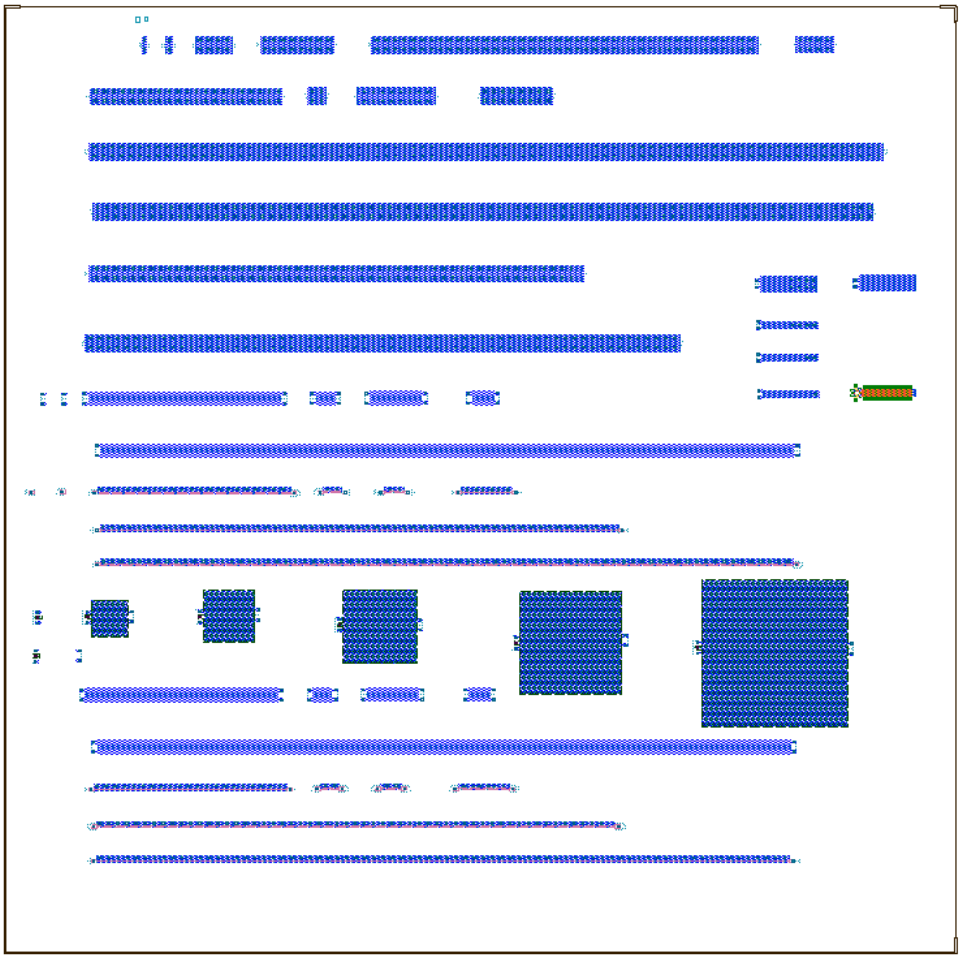

Figure 3.4. Layouts of test structures including the transmission lines and capacitors.

After fabricating the designed test structures, the scattering parameters of our designed structures were measured using a 50 ohm probe station VNA from 100 MHz to 10 GHz. Ultimately, the LTCC dielectric characteristics such as the characteristic impedance, attenuation constant, effective dielectric constant and loss tangent will be calculated based on the Conformal Mapping Technique Calculations using the measured scattering parameters [42].

3.3.1 CBCPW Electromagnetics Simulation

The CBCPW formulas will be disscussed in details in Section 3.4.1. A 50 ohm, 10150 µm CBCPW is shown in Figure 3.5. We utilized ADS EM simulator to obtain the scattering parameters, and the smith chart shown in Figure 3.6 which confirm the 50 ohm matching from dc to 10 GHz frequency range.

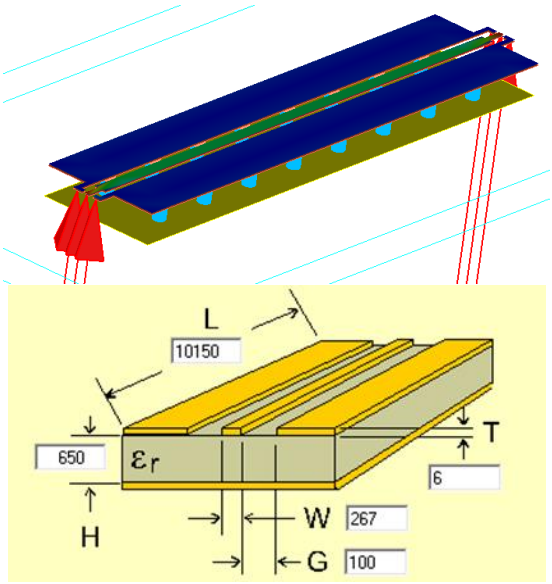

Figure 3.5. Designed 50 ohm sample CBCPW with *W*=246 µm, *l*=10150 µm, *G*=100 µm, we have considered the Dupont 951 technology: *T*=6 µm, *H*=6*100 µm, σ=6.3*e+07 S/m and "*κ*"=7.99.

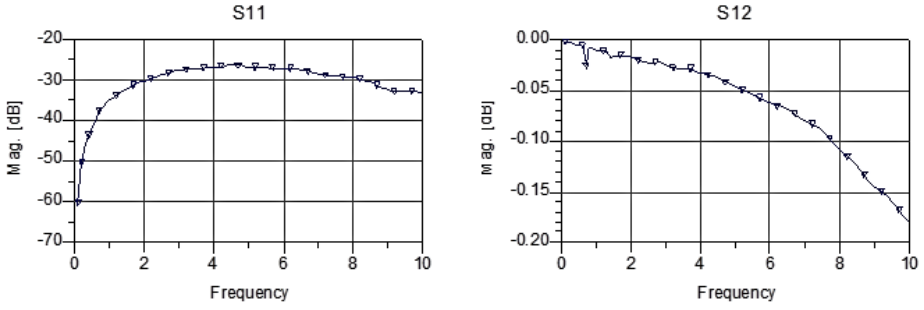

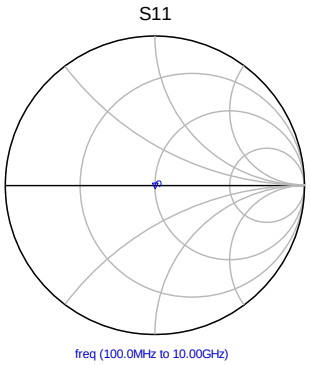

Figure 3.6. Scattering parameters and smith chart of CBCPW.

3.3.2 Stripline Electromagnetics Simulation

The formulas for the stripline were discussed in detail in Section 2.4.2. Figure 3.7 shows a 50 ohm, 10150 µm stripline that was designed using App CAD software. ADS EM simulator was utilized to obtain the scattering parameters and the smith chart shown in Figure 3.8 which confirm the 50 ohm matching from dc to 10 GHz frequency range.

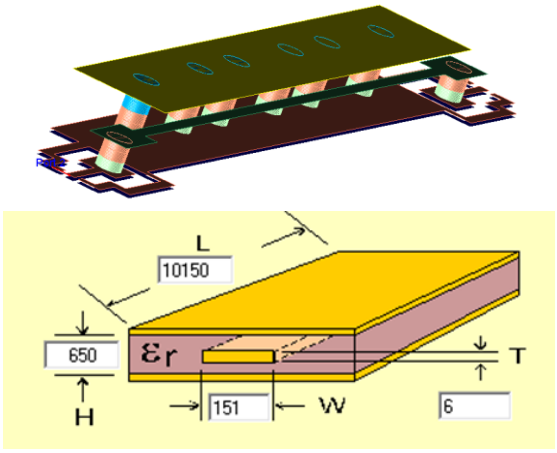

Figure 3.7. Designed 50 ohm sample stripline with *W*=151 µm, *l*=10150 µm, we have considered the supplier technology: *T*=6 µm, *H*=6*100 µm, σ=6.3*e+07 S/m and "*κ*"=7.99.

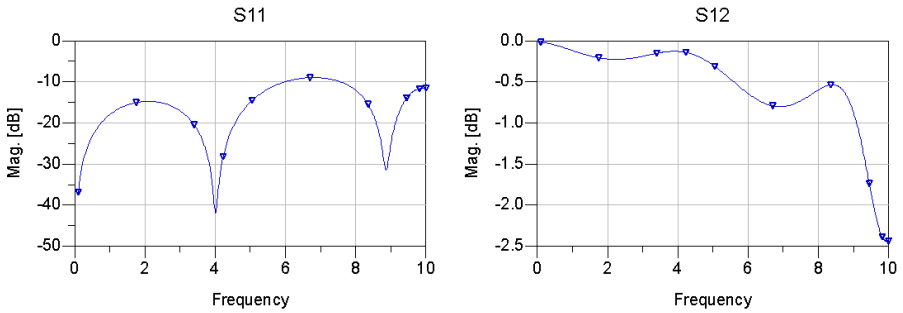

Figure 3.8. Scattering parameters of stripline.

3.3.3 Microstrip Electromagnetics Simulation

The microstrip forumlas for this simulation was already discussed in detail in Section 2.4.3. Figure 3.9 shows a 50 ohm, 1150 µm stripline that was designed using App CAD software. The scattering parameters and the smith chart shown in Figure 3.10 were obtained from ADS EM simulations which confirm the 50 ohm matching from dc to 10 GHz frequency range.

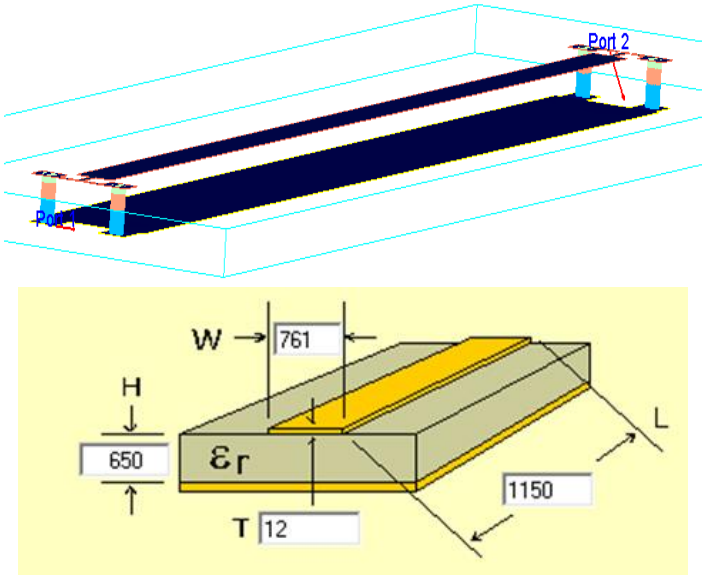

Figure 3.9. Designed 50 ohm sample microstrip with *W*=761 µm, *l*=1150 µm, we have considered the supplier technology: *T*=6 µm, *H*=6*100 µm, σ=6.3*e+07 S/m and "κ"=7.99.

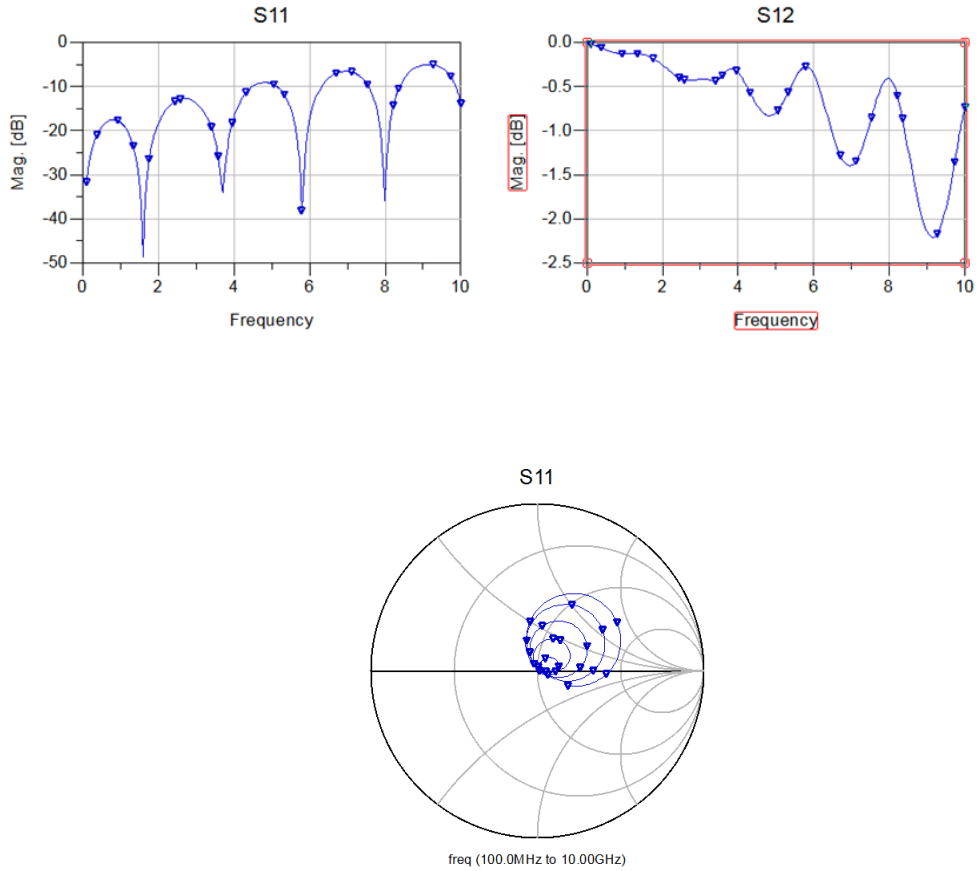

Figure 3.10. Scattering parameters and smith chart of microstrip.

From the simulated scattering parameters of the CBCPW sample, stripline and microstripline shown in Figure 3.5 through Figure 3.10, it is confirmed that they offer 50 ohm matching over the entire frequency band of 1GHz to 10 GHz. Table 3.3 summerizes the design parameters of the final fourteen CBCPWs. *W* is the signal line width, *S* defines the seperation space between the signal and the ground lines, *Wg* is the ground line width, *H* is the width of the six layer LTCC substrate, *t* denotes the conductor's thickness dictated by the Dupont 951 design rules and *L* is CBCPW lengths designed according to [24].

Table 3.3. Design parameters of CBCPWs with ground plane.

W-S-Wg(um)	t(um), H(um)	L(mm)
246,100,1000	6,600	0.650
246,100,1000	6,600	1.150
246,100,1000	6,600	5.150
246,100,1000	6,600	10.150
246,100,1000	6,600	53(1ghz)
246,100,1000	6,600	5.3(10ghz)
246,100,1000	6,600	26.5(1ghz)
246,100,1000	6,600	2.65(10ghz)
246,100,1000	6,600	109(1ghz)
246,100,1000	6,600	107(1ghz)
246,100,1000	6,600	10.8(10ghz)
246,100,1000	6,600	100(10ghz)
246,100,1000	6,600	68(1ghz)
246,100,1000	6,600	81.6(1ghz)

3.4 Dielectric Constant and Loss Tangent Calculations

3.4.1 Dielectric Constant

The dielectric constant (ε_r) is the ratio of the permittivity of a substance ($\varepsilon_{material}$) to the permittivity of free space (ε_0). The dielectric constant is a bulk material property, while the effective dielectric constant is a parameter that depends on the transmission line geometry.

The propagation constants of a CBCPW can be related to the measured S_{21} by

$$\alpha = -\frac{S_{21}(dB)}{l(cm)}$$

$$\beta = -\frac{\Delta\varphi_{S_{21}}(deg)}{l(cm)}, \qquad (3.3)$$

where, α denotes the attenuation constant in decibel per centimeter (*dB/cm)*, β is the phase constant in *cm-1* and $\Delta\Phi S_{21}$ is the phase shift of the transmission coefficient S_{21} ,while *l* is the transmission line length in centimeters. $\Delta\Phi S_{21}$ is related to the effective dielectric constant ε_{eff} by

$$\Delta\varphi_{S_{21}} = -\frac{2\pi f.l.\sqrt{\varepsilon_{eff}}}{c}. \qquad (3.4)$$

From the effective dielectric constant values, the relative dielectric constant of the LTCC dielectric material and the characteristic impedance of the lines are extracted using analytical expressions based on the quasi-TEM approach [43].

The approximate Conformal Mapping Technique [28] gives the effective dielectric constant as

$$\varepsilon_{eff} = \frac{1 + \varepsilon_r . \frac{K(k')}{K(k)} . \frac{K(k1)}{K(k'1)}}{1 + \frac{K(k')}{K(k)} . \frac{K(k1)}{K(k'1)}}, \quad (3.5)$$

and characteristic impedance as

$$Z_0 = \frac{60\pi}{\sqrt{\varepsilon_{eff}}} . \frac{1}{\frac{K(k)}{K(k')} + \frac{K(k1)}{K(k'1)}}, \quad (3.6)$$

where *K* is the complete elliptic integral of the first kind [43], and *K'* is its complementary function,

$$K'(k) = K(k'), with\ k' = \sqrt{1 - k^2}$$

$$k_0 = \frac{W}{W + 2S}$$

$$k_1 = \frac{\tanh(\frac{\pi W}{4H})}{\tanh[\frac{\pi(W+2S)}{4H})}$$

$$k_0{}' = \sqrt{1 - k_0{}^2} \text{ and } k_1{}' = \sqrt{1 - k_1{}^2},$$

for *0<k<0.7070* and *0<K/K'<1*

$$\frac{K(k)}{K(k')} \approx \pi / \ln[2\frac{1+\sqrt{k'}}{1-\sqrt{k'}}]$$

$$\frac{K(k)}{K'(k)} \approx \pi/\ln[2\frac{1+\sqrt{k}}{1-\sqrt{k}}]$$

where,ε_r is the dielectric constant of the LTCC film, *H* is the film's thickness, *S* denotes the spacing to the adjacent ground, and *W* is the trace width. H_{total}*=600* μm, *W=240* μm, and *S=100* μm.

We utilized MATLAB for solving the elliptic functions.

3.4.2 Loss Tangent

The CPW transmission line can also be described in terms of its distributed resistance, inductance, capacitance and conductance *(R, L, C, G),* given by

$$R + j\omega L = \gamma Z_0$$

$$G + j\omega C = \gamma / Z_0$$

$$tan\delta = \frac{G}{\omega C}, \qquad (3.7)$$

where *C* and *G* are given by the relations

$$C = \frac{Im\left[\frac{\gamma}{Z_0}\right]}{\omega}$$

$$G = Re\left[\frac{\gamma}{Z_0}\right],$$

where $\gamma = \alpha + j\beta$.

3.5 Measurement

After fabricating the designed test structures, the scattering parameters were measured using a 110 GHz Vector Network Analyzer with a 50 ohm probe station in a Microwave to Millimeter Wave Laboratory located at the Electrical and Computer Engineering Research Facility (ECERF) at the University of Alberta as shown in Figure 3.11.

Figure 3.11. VNA probe station at M2M.

3.5.1 Measurement versus Simulation

Figure 3.12 shows the test structures fabricated by ACAMP on Dupont 951 LTCC.

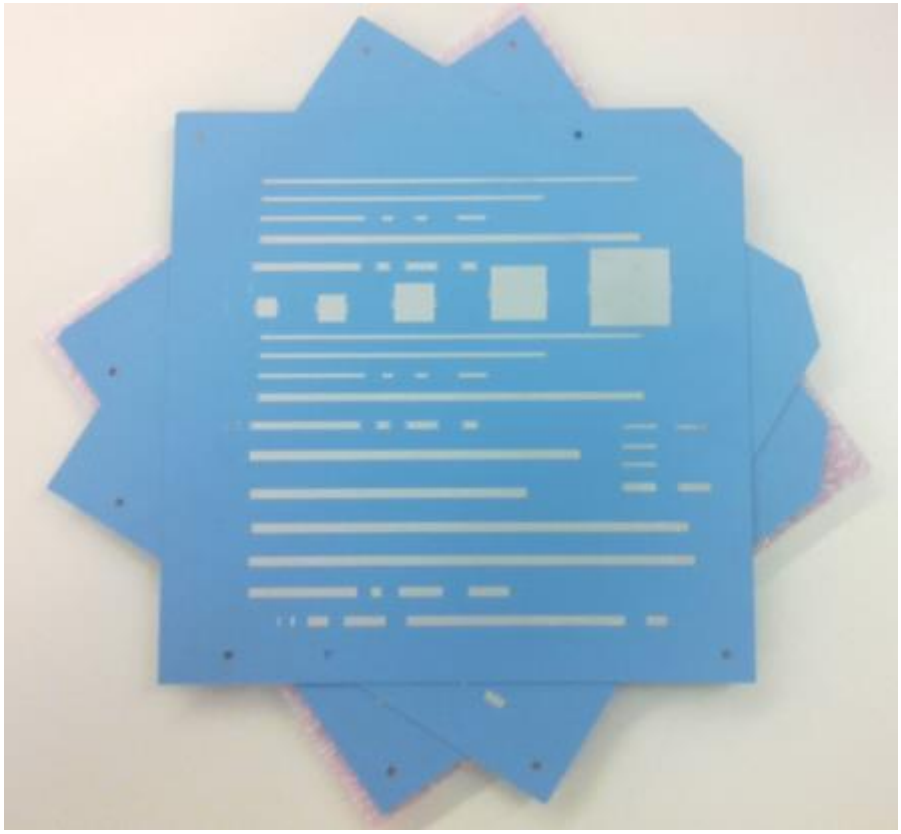

Figure 3.12. Test structures fabricated by ACAMP on Dupont 951 LTCC.

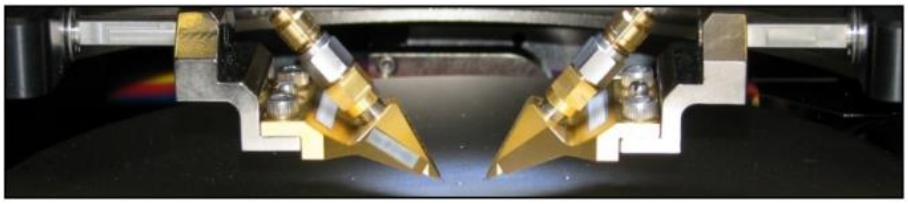

Figure 3.13. 50 ohm miniature Z probe pitch of the VNA.

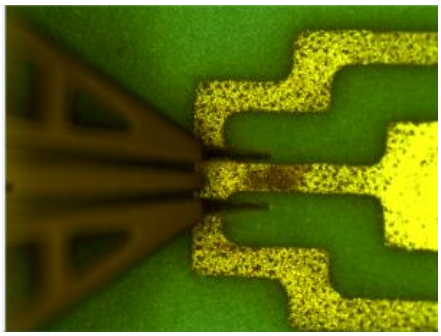

Figure 3.14. Input port of a stripline to be measured under VNA's microscope.

Figure 3.14 shows the input port of one of the striplines to be measured using a 50 ohm probe station under a VNA's microscope.

To ensure the proper testing of our test structures in the required frequency range , the measured scattering parameters of the test structures were imported to an ADS EM simulator through the "S2P" instance file. A comparision of the measured results and the scattering parameters from the ADS EM simulations were done for our model verification as demonstrated in Figure 3.15.

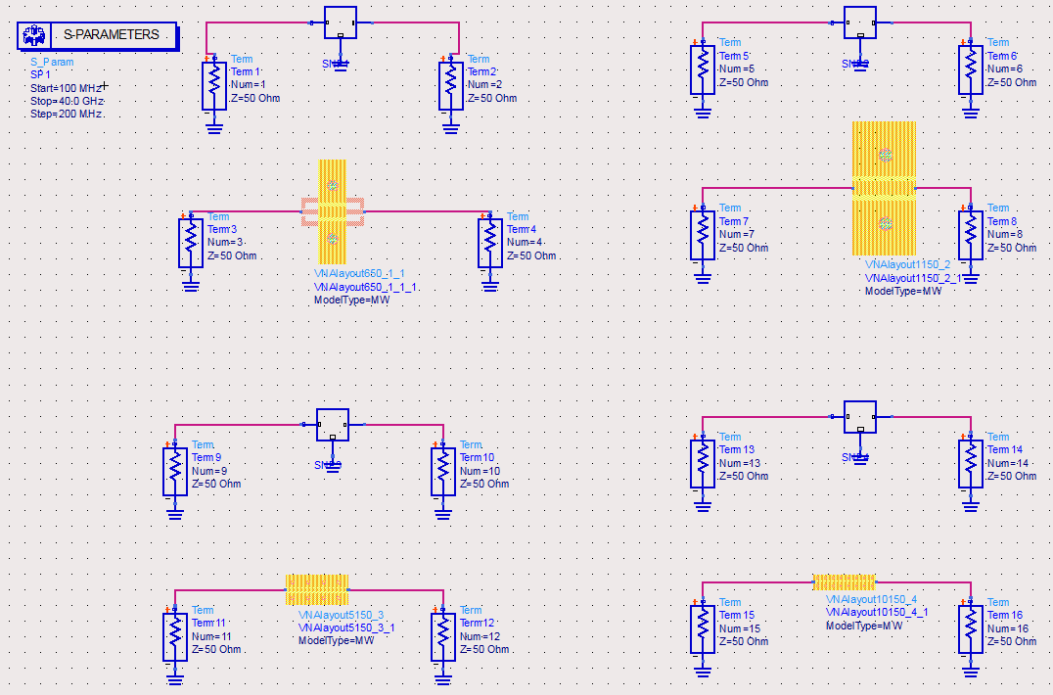

Figure 3.15. ADS file to compare measurement results and Electromagnetic simulation data.

Figure 3.16 through Figure 3.27 show the ADS EM simulation results of the scattering parameters' phase and amplitude in degree and decibel for 650 µm, 1150 µm, 5150 µm and 10150 µm CBCPW lines. The measured scattering parameters of the mentioned transmission lines are illustrated on the charts for comparison purposes.

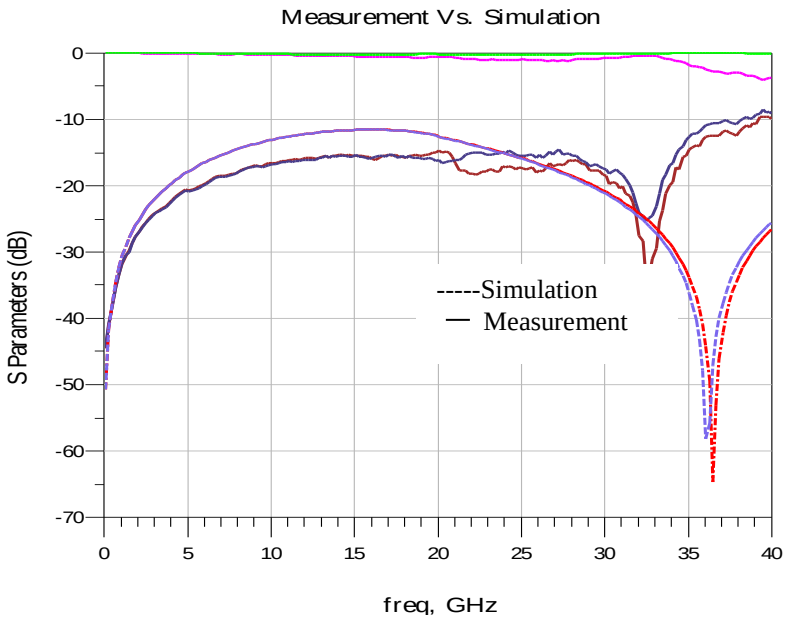

Figure 3.16. Measured and simulated scattering parameters of the 650 µm CBCPW.

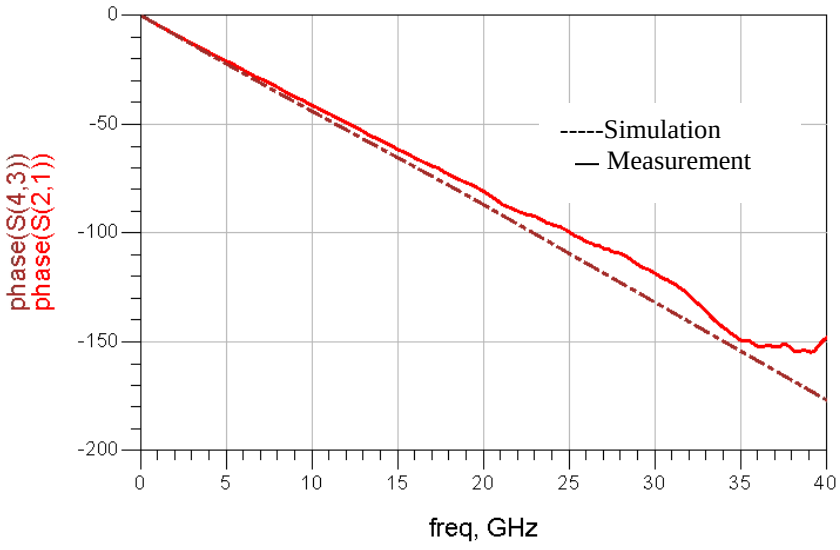

Figure 3.17. Measured and simulated $\Delta\Phi S_{21}$ of the 650 µm CBCPW.

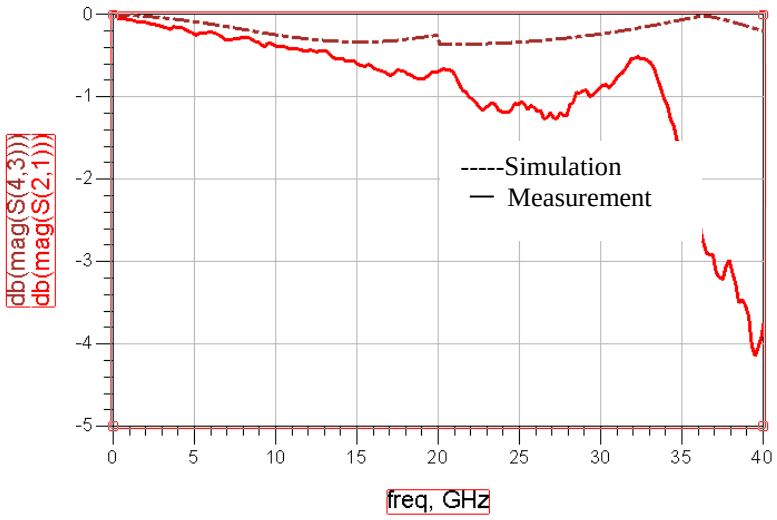

Figure 3.18. Measured and simulated S_{21} magnitude of the 650 µm CBCPW.

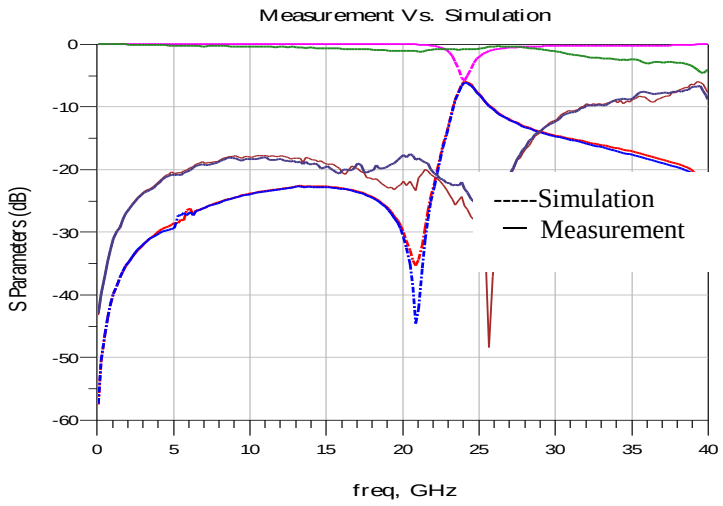

Figure 3.19. Measured and simulated scattering parameters of the 1150 µm CBCPW.

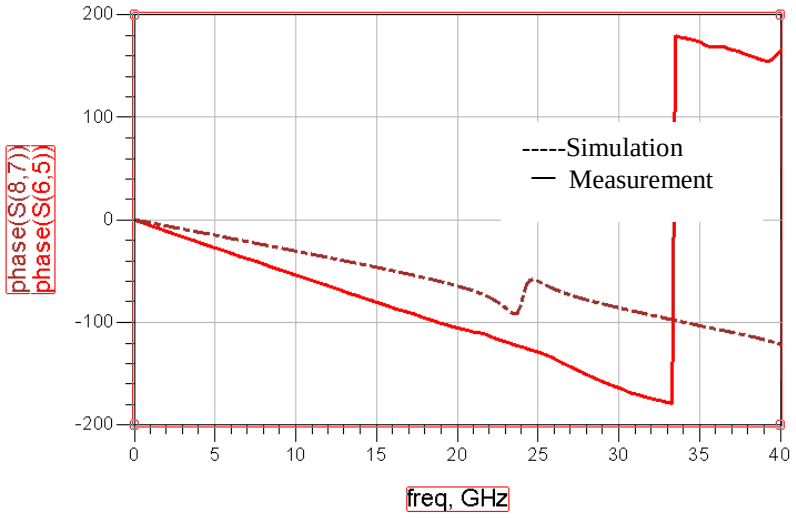

Figure 3.20. Measured and simulated $\Delta\Phi S_{21}$ of the 1150 µm CBCPW.

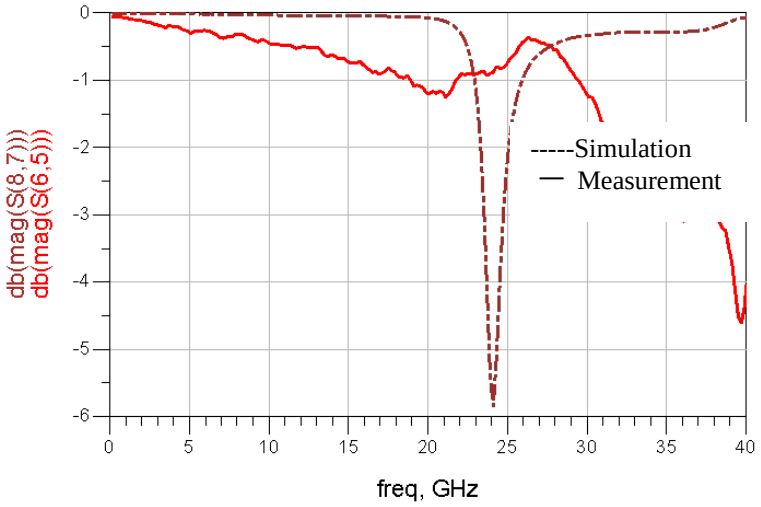

Figure 3.21. Measured and simulated S_{21} magnitude of the 1150 µm CBCPW.

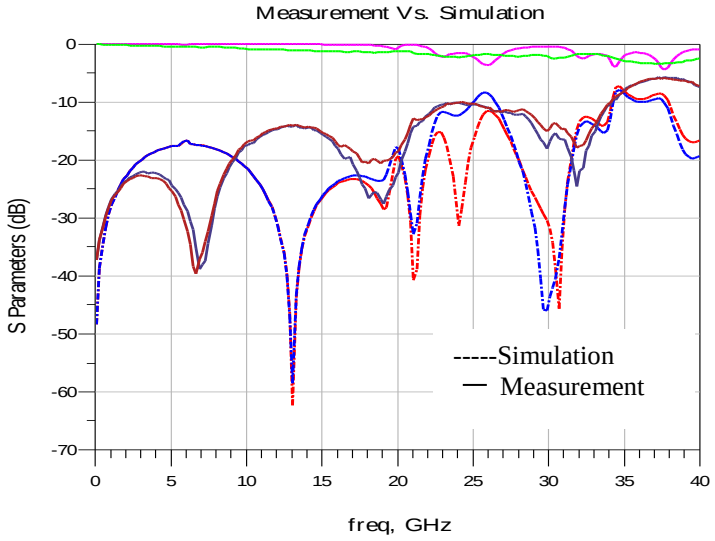

Figure 3.22. Measured and simulated scattering parameters of the 5150 µm CBCPW.

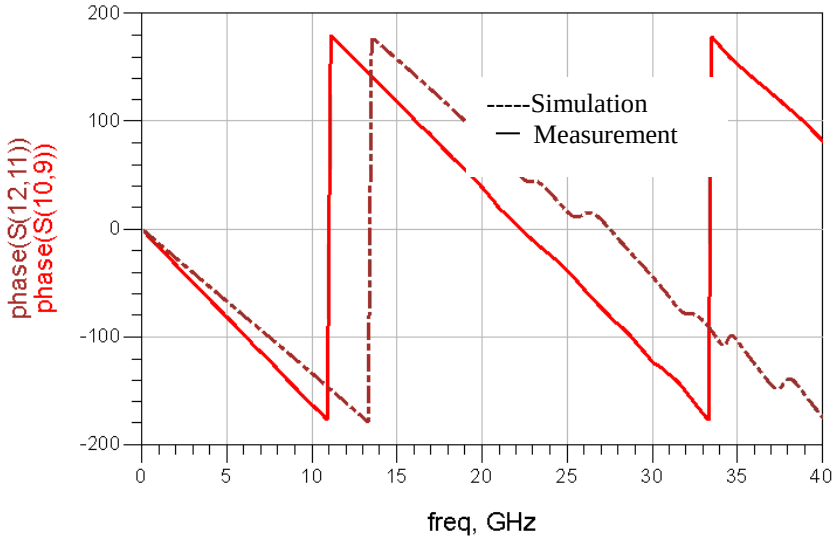

Figure 3.23. Measured and simulated $\Delta\Phi S_{21}$ of the 5150 µm CBCPW.

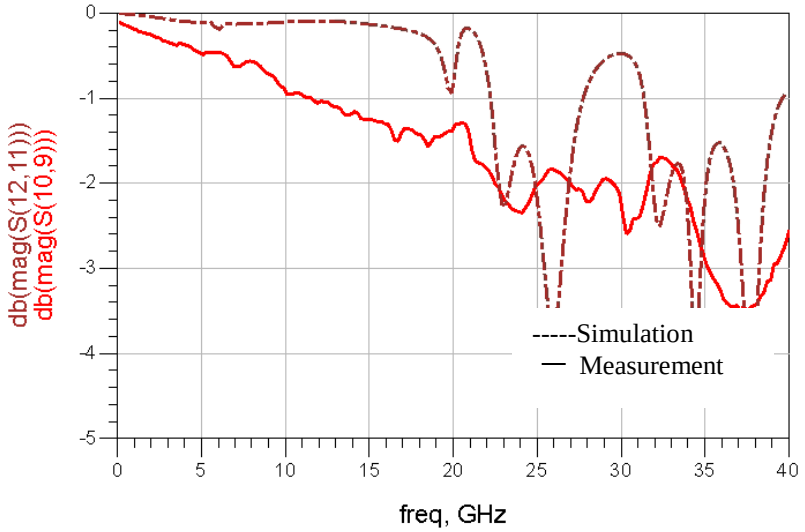

Figure 3.24. Measured and simulated $\Delta\Phi S_{21}$ of the 5150 µm CBCPW.

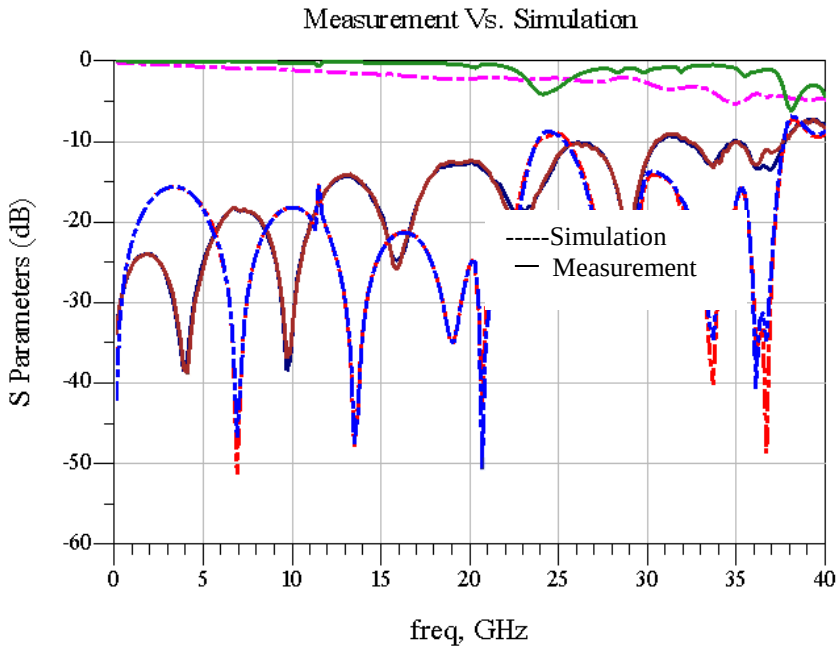

Figure 3.25. Measured and simulated scattering parameters of the 10150 µm CBCPW.

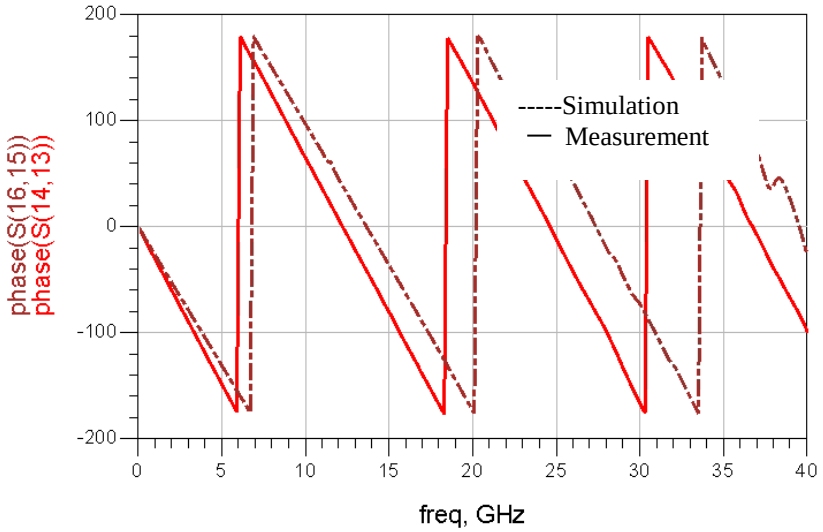

Figure 3.26. Measured and simulated $\Delta\Phi S_{21}$ of the 10150 µm CBCPW.

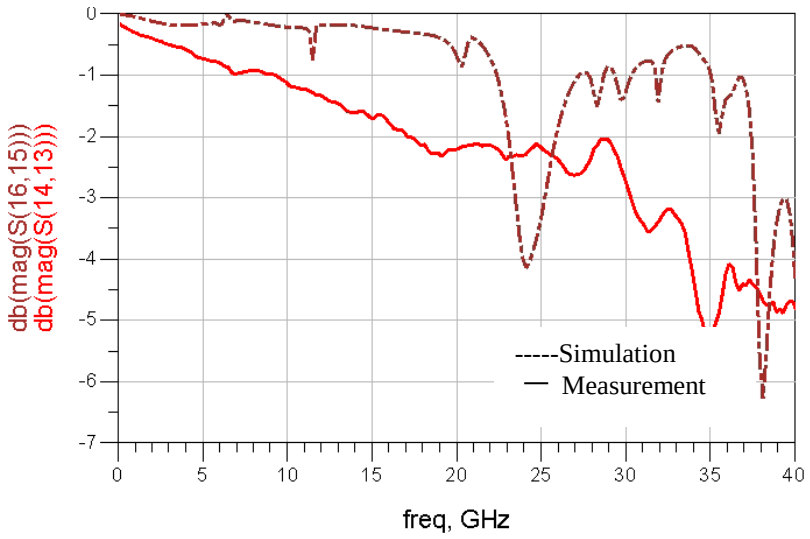

Figure 3.27. Measured and simulated S_{21} magnitude of the 10150 µm CBCPW.

As shown from Figures 3.16 through 3.27, the difference between the measured and simulated results confirm the nessecity of de-embedding the transmission lines, which will be described in the following section.

3.6 De-embedding DUT

An accurate characterization of the surface mount Device Under Test (DUT) requires the test fixture characteristics to be removed from the measured results which includes the effects of the coaxial interfaces, the VNA and the ports of the transmission lines [44].

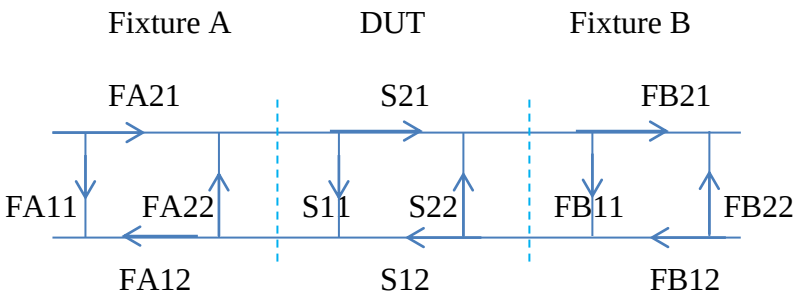

Figure 3.28. Signal flow graph representing the test fixture halves and the Device Under Test (DUT) [44].

If we consider the test fixture and DUT as three cascaded networks and use the T-parameter matrix, we can conclude

$$[T_{Measured}] = [T_A][T_{DUT}][T_B]. \qquad (3.8)$$

The resulted matrix represents the T-parameters of the test fixture and the DUT measured by the VNA. Our goal is to de-embed the two sides of the fixture, T_A and T_B, and gather the information from the DUT. So we should multiply each side of the measured results by the inverse T parameter matrix of the fixture which yields to the T-parameter of the DUT itself

$$[T_A]^{-1}[T_A][T_{DUT}][T_B][T_B]^{-1} = [T_{DUT}]. \qquad (3.9)$$

The T-parameter matrix can then be converted back to the desired S-parameter matrix [45] using

$$S_{11}=T_{21}/T_{11} \qquad S_{12}=(T_{11}T_{22}-T_{12}T_{21})/T_{11} \qquad (3.10)$$

$$S_{21}=1/T_{11} \qquad S_{22}=-T_{12}/T_{11}.$$

To remove the test fixture characteristics from the transmission lines, we have to de-embed the effects of the ports. For de-embedding purposes we have designed dummy ports exclusively for each test structure so that we can measure their scattering parameters and de-embed them from the transmission lines' scattering parameter measurements. Since our dummy ports are designed as one port, we need to write a MATLAB code to convert the one port dummy T parameters to its equivalent two-port dummy T parameters.

Using the formulas above, we are able to de-embed the test fixture effects and calculate the dielectric properties of the LTCC substrate precisely.

In the following section we will describe how to model the ports properly.

3.6.1 Modeling Port as a RLC Network

Intially, we modeled the ports of our designed test structures with a parrallel capacitor to the ground. This model was not accurate enough to demonstrate reasonable results. Measuring the real part of the port impedance as shown in Figure 3.29 confirmed the existance of a resistive part in the port, consequently we modeled the transmission line port as a RLC circuit as shown in Figure 3.30.

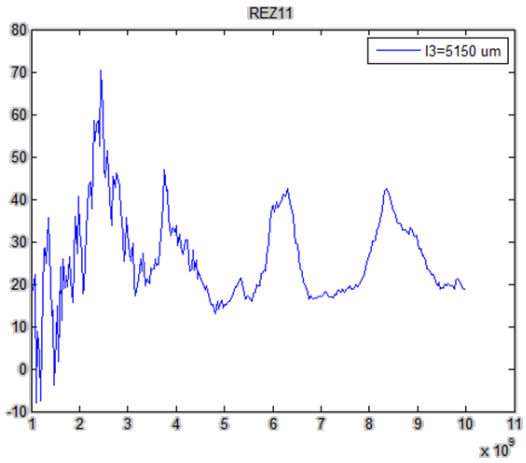

Figure 3.29. Measured real part of the port impedance.

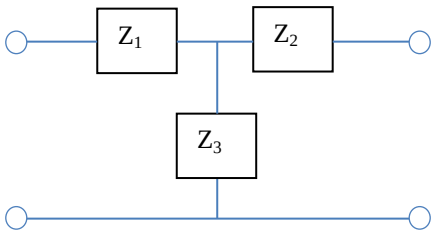

Figure 3.30. RLC model for the transmission line's ports [46].

Figure 3.30 shows the RLC model for the transmission line's ports, where $Z_1=R$, $Z_2= jwL$ and $Z_3= 1/jwC$ [49]. If we write the ABCD-Parameters of the circuit in Figure 3.30, we will have

$$A=1+Z_1/Z_3 \qquad B=Z_1+Z_2+Z_1Z_2/Z_3 \qquad (3.11)$$

$$C=1/Z_3 \qquad D=1+Z_2/Z_3 .$$

Then we will convert the ABCD-Parameters to S-Parameters [50] using

$$S_{11}=(A+B/Z_0-CZ_0-D)/(A+B/Z_0+CZ_0+D)$$

$$S_{12}=(2(AD-BC))/(A+B/Z_0+CZ_0+D)$$

$$S_{21}=2/(A+B/Z_0+CZ_0+D)$$

$$S_{22}=(-A+B/Z_0-CZ_0+D)/(A+B/Z_0+CZ_0+D). \quad (3.12)$$

Ultimately, when we convert the S-parameters to the T-parameters it will lead to

$$T_{11}=1/S_{21} \qquad T_{12}=-S_{22}/S_{21} \quad (3.13)$$

$$T_{21}=S_{11}/S_{21} \qquad T_{22}=(S_{12}S_{21}-S_{11}S_{22})/S_{21}.$$

Now we can use the de-embedding formulas described in Section 3.6 and extract the T-parameters of our DUT. Converting the T-parameters back to S-parameters will give us the de-embedded measurement results of our test structures. Now we can utilize the Conformal Mapping Technique [46] described in Section 3.4 to characterize the LTCC and calculate the dielectric constant and loss tangent.

3.6.2 Simulation Results

In this section, to verify the necessity of de-embedding the effect of the ports, we will compare the measured and simulated results of the test structures before and after de-embedding. Figures 3.31 shows the dielectric constant of LTCC based on ADS EM simulations,while Figure 3.32 and 3.33 illustrate the dielectric properties of the LTCC based on the measurement results up to 10 GHz before de-embedding the test fixture from our test structures. As shown, there is a signifinacnt discrepenacy between the dielectric constant and the loss tangent of two structures.

Figure 3.34 and 3.35 show the calculated dielectric constant and loss tangent of the LTCC based on the comformal mapping tecnique using the de-embedded scattering parameter measurement results of the CBCPWs. The de-embedded results confirm that the measuremnt and simulation results follow each other closely.

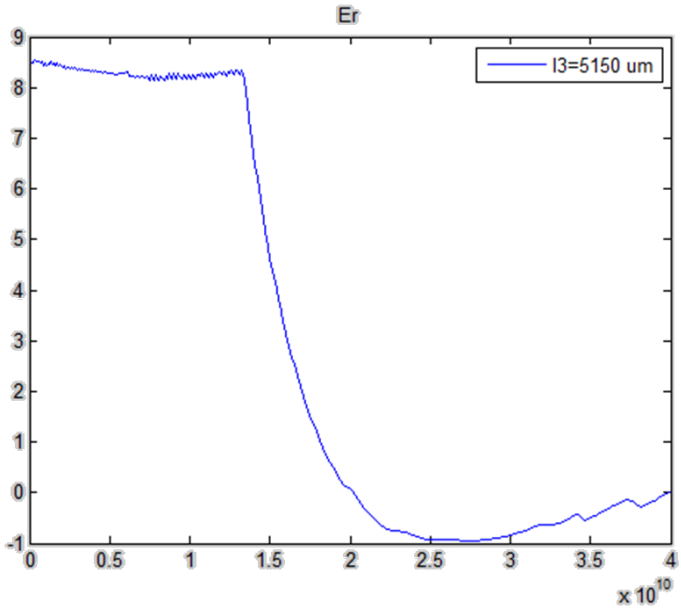

Figure 3.31. Dielectric constant of the LTCC using the ADS simulation results up to 40 GHz.

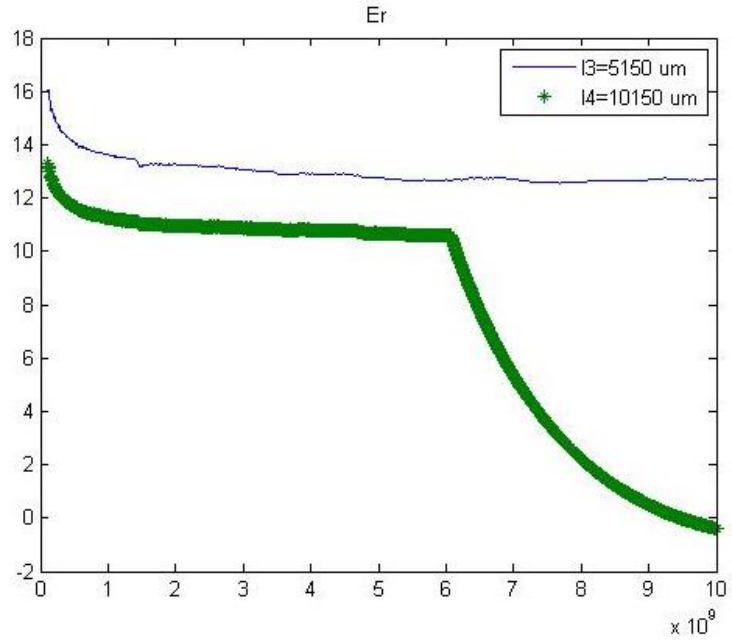

Figure 3.32. Dielectric constant of the LTCC using the measurement results before de-embedding up to 10 GHz.

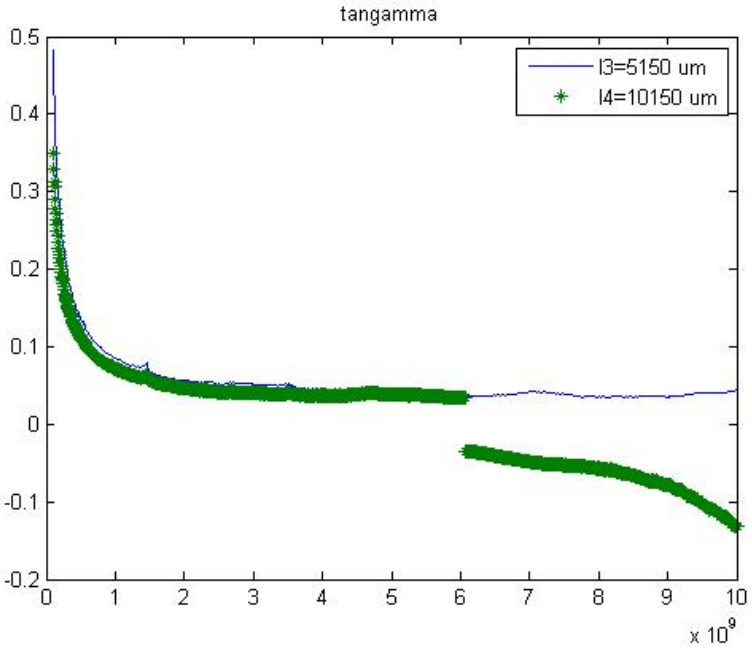

Figure 3.33. Loss tangent of the LTCC using the measurement results before de-embedding up to 10 GHz.

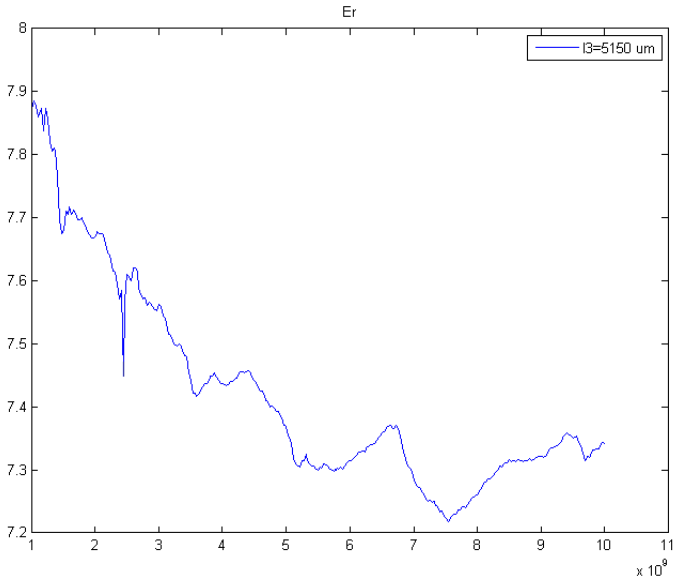

Figure 3.34. Dielectric constant of the LTCC using the measurement results after de-embedding up to 10 GHz.

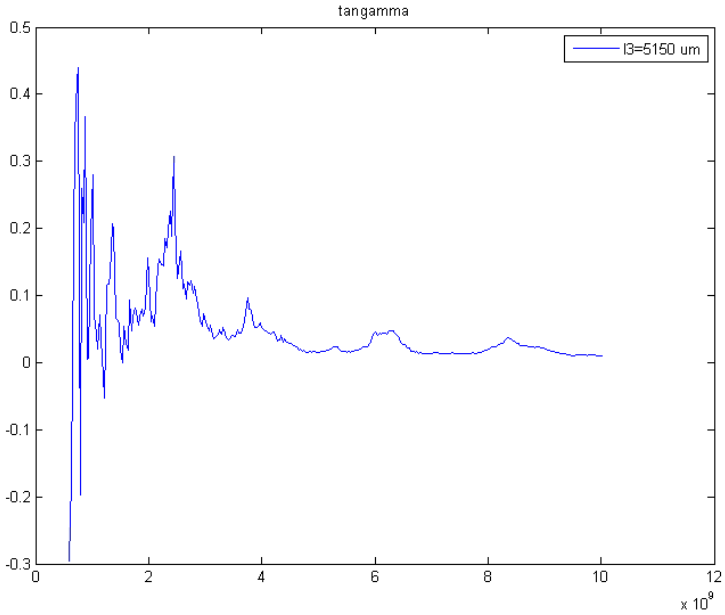

Figure 3.35. Loss tangent of the LTCC using the measurement results after de-embedding up to 10 GHz.

Finally, after de-embedding the CBCPW ports, the dielectric constant and loss tangent are calculated using the method described in this chapter. Table 3.4 denotes the dielectric properties of the LTCC at eleven discrete frequencies.

Table 3.4. Loss tangent and dielectric constant of LTCC.

Frequency GHz	Dielectric Constant	Loss Tangent
0.5	8	0.1
1	7.8	0.02
2	7.6	0.01
3	7.5	0.06
4	7.4	0.05
5	7.3	0.01
6	7.3	0.04
7	7.3	0.01
8	7.3	0.02
9	7.3	0.02
10	7.3	0.01

3.7 Summary

In Chapter 3 we designed five parallel plate capacitors and fourteen CBCPWs using Agilent App CAD and ADS EM simulations to characterize the Dupont 951 LTCC substrate from 100 MHZ to 10 GHz. To obtain the scattering parameters of the CBCPW test structures, the effects of the pads are de-embedded from the

measured scattering parameters using a conventional de-embedding method. In order to de-embed the test fixture we needed to model the ports of our test structure designs as two port RLC circuits using MATLAB software. Finally the dielectric constant and loss tangent were calculated accurately, utilizing the Conformal Mapping Technique.

Chapter 4

Proposed De-Embedding Method

In this chapter, we will present a new de-embedding method for removing the effect of the test fixtures, such as the pads, on the scattering parameters of the device under test. The proposed method not only de-embeds the pad but also certain lengths of the transmission line connecting the pads to the device under test leaving the electromagnetic field around de-embedded structure relatively unchanged from that of the original structure. This will produce more accurate measurement results for a de-embedded structure, and consequently a more accurate characterization of the material.

Section 4.1 introduces the proposed de-embedding method. Then, we will develop the theory of the method in Section 4.2. The properties of reciprocal and non-reciprocal networks will be studied in 4.3 to facilitate the calculation of the scattering parameters of the de-embedded structure.

In Section 4.4, we will compare the electromagnetic fields of the de-embedded test structure and the original test structure to prove the improvement in the proposed method compared to the conventional de-embedding methods. Finally,

the numerical results for the dielectric constant and loss tangent of the LTCC material obtained based on the proposed de-embedding technique will be illustrated in Section 4.5. Chapter 4 is summarized and concluded in Section 4.6.

4.1 Introduction

It is necessary to de-embed the effect of the test fixtures such as the pads on the DUT's measured scattering parameters to obtain its own scattering parmameters. In the convetional de-embedding method, the scattering paramaters of the pads are removed by measuring the single-port scattering parmaters of the dummy pads that are implemented and tested along with the device under test. The input pad, the de-embedded DUTand the output are considered to be three cascaded blocks, this means the overall transmission parmaters of the non-embedded structure can be written as

$$T_{overall} = T_{input\_pad} \cdot T_{de-embedded\_DUT} \cdot T_{output\_pad}. \quad (4.1)$$

and the scattering parameters of the de-embedded DUT can be obtained by

$$T_{de-embedded\_DUT} = T_{input\_pad}^{-1} \cdot T_{overall} \cdot T_{output\_pad}^{-1}. \quad (4.2)$$

This method assumes that the electromganetic enviroment arount the de-embedded DUT is the same as the overall DUT including the pads. However, in many cases, the size of the pads is in the same scale as the DUT and their effects on the electrogmanetic fields in the vicinity of the DUT can not be negelected.

Therefore, the resulting scattering parmaters based on the above equation does not accurately represent the scattering parameters of the DUT if we were able to test it without pads.

In order to obtain accurate results related only to the de-embedded DUT, we propose that part of test structure and the pads be de-embedded from the measurement results, instead of only removing the effect of the pads. This will leave some distance between the pad and the actual DUT, thus mininizing the effect of the pads on the electromganetic fields around the DUT. Of course, this method requires that the part of test structure and the pads be constructed as a dummy test fixture along with the device under test. Illustrated in Figure 4.1, the middle DUT represents the de-embedded transmission line using the conventional methods while the lower DUT demonstrates the de-embedded transmission line using the proposed de-embedding method.

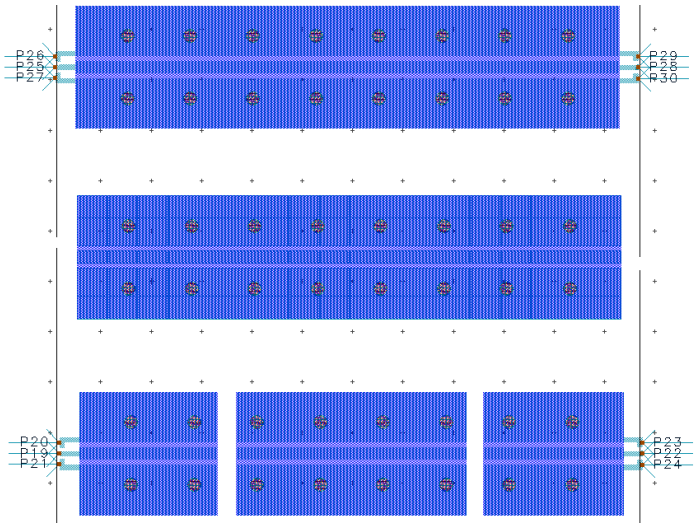

Figure 4.1. Conventionally de-embedded transmition line in the middle and the proposed de-embedded line at the bottom.

4.2 Theory of Proposed De-embedding Method

In this section, we will apply the proposed de-embeeding method to our dielectric charatrization applications.We have selected the designed 5000 µm CBCPW as our main test structure to be measured to extract the dielectric constant and loss tangent of the LTCC substrate. Using our RF probes that have a 100 µm pitch, the designed CBCPW lines are connected to the the specially designed input and output ports in order to be able to measure the s-parameters of the 5000 µm CBCPW lines. This set up is shown in Figure 4.2.

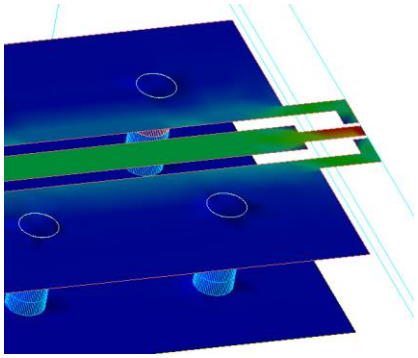

Figure 4.2. 5150 µm CPW transmission line including input and output ports, *W*=246 µm, *l*=5150 µm, *G*=100 µm, *T*=6 µm, *H*=6*100 µm, σ=6.3*e+07 S/m and "κ"=7.99.

However, the designed port will change the electrogmanetic field in the vicinity of the 5000 µm CBCPW, leading to inaccurate results if the structure is tested this way. Therefore, in order to minimize the effect of port on the electromagnetic field around the 5000µm CBCPW, we have added two 2575µm CBCPW sections

with exactly similar structures as the original 5000μm CBCPW line to both ends of the DUT. Then, we fabricated and measured the scattering parmaters of a 10150μm CBCPW line to be used for accurate charaterization of a 5000 μm CBCPW line. In addition, we needed to fabricate our test fixture, a 2575 μm CBCPW line connected to the port, and measure its scattering parameters making it possible to de-embed their effect on the scattering parmaters. In order to meausre the two-port scattering parameters, we constructed two back-to-back 2575 μm structures to form a 5150 μm CBCPW with input and output ports.

4.3 Electromagnetic Field Comparison

In Section 4.3, we will confirm that in order to obtain accurate results related only to the de-embedded DUT, parts of test structure in addition to the pads should be de-embedded from the measurement results. This will leave some distance between the pads and the actual DUT, minimizing the effect of pads on the electromagnetic fields around the DUT.

We will compare the similarities and discrepancies of the electromagnetic field distributions of a CPW in the vicinity of pads and in some distance from the pads.

We can visualize the electric field and the magnetic field of CPWs using ADS FEM simulator.

Figure 4.3 shows CPW Electric-E and Magnetic-H field distributions in theory; the solid lines show electric field of the CPW while the dashed lines demonstrate its magnetic field.

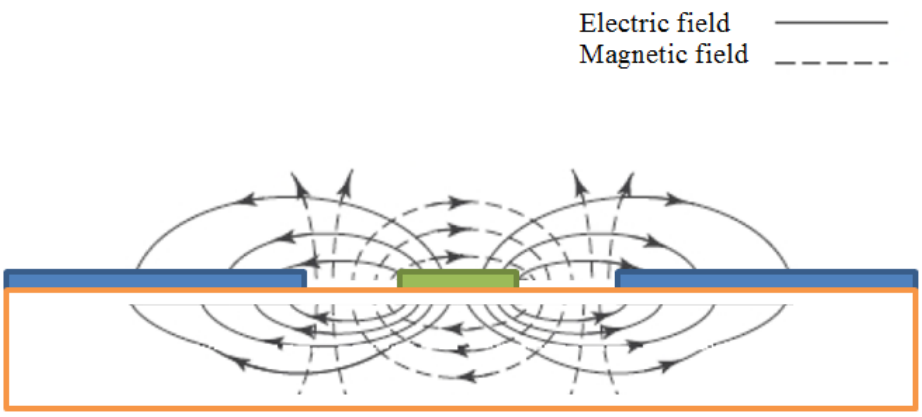

Figure 4.3. CPW Electric-E and Magnetic-H field distribution.

Figure 4.4.a shows the electric field distribution of a short CBCPW with physical ports and Figure 4.4.b visualizes its magnetic field distribution using an ADS FEM simulator. As can be seen, there is a significant discrepancy in the electromagnetic fields in the vicinity of the physical ports of the CBCPW, this will result in less accurate calculations of the material characterization if we de-embed the DUT conventionally.

Figure 4.5.a shows the electric field distribution of the 10150 µm CBCPW with physical ports and Figure 4.5.b visualizes its magnetic field distribution using an ADS FEM simulator. If we de-embed some parts of the transmission line in addition to the ports as described in details earlier, we will have much more similar electromagnetic fields to the original line. This will produce more accurate measurement results for a de-embedded structure, and consequently a more accurate characterization of the LTCC material.

The red color in Figure 4.4 and 4.5 represents the regions with maximum voltage while the green color visualizes the regions bearing the average voltage and the blue regions have zero voltage.

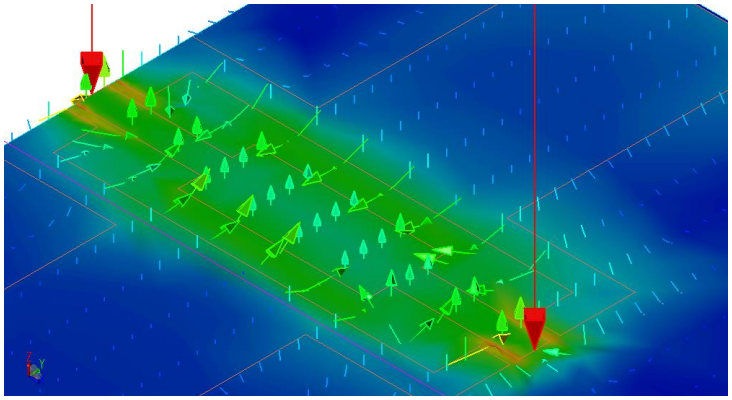

(a)

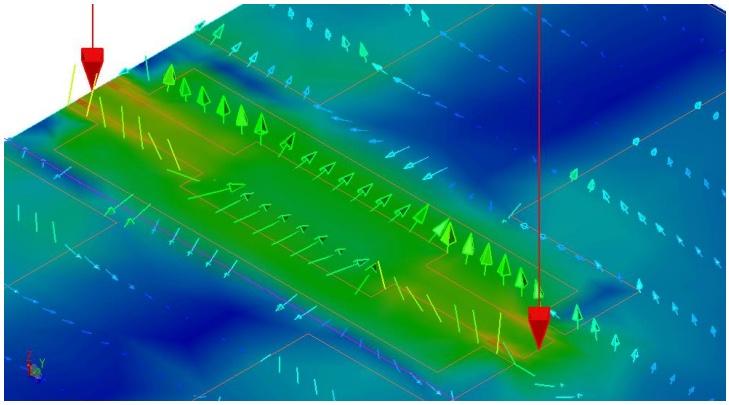

(b)

Figure 4.4. (a) Electric field distribution of a 650 µm CBCPW, (b) Magnetic field distribution of a 650 µm CBCPW.

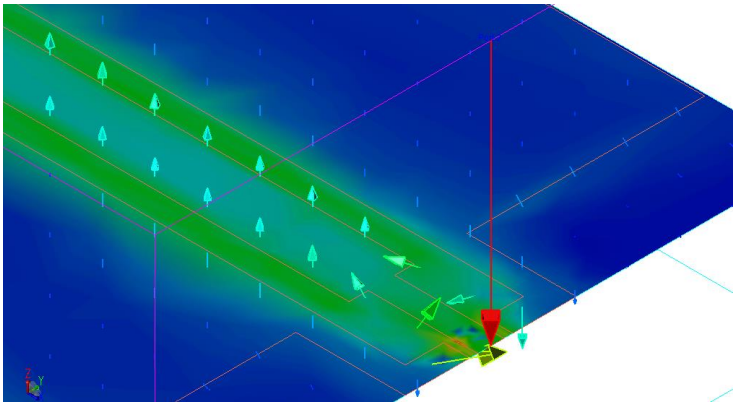

(a)

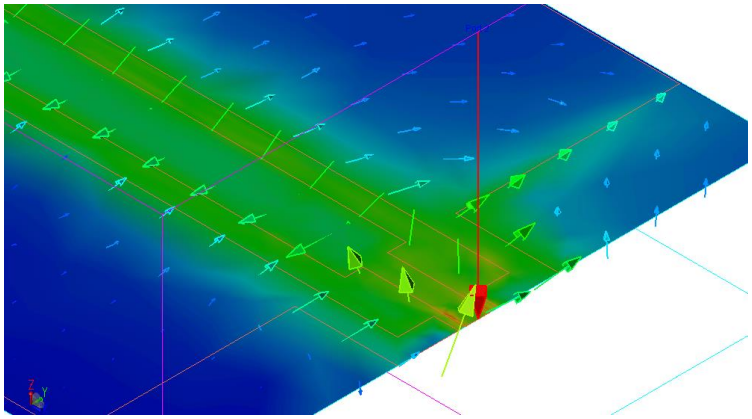

(b)

Figure 4.5. (a) Electric field distribution of 10150 CBCPW, (b) Magnetic field distribution of 10150 CBCPW.

4.4 Characterization of Test Fixtures

After fabricating the designed 5150 µm CBCPW structure, we measured its scattering parameters using a 110 GHz VNA through a 50 Ohm probe station. The results were used to obtain the scattering parameters of our test fixture, a 2575 µm CBCPW connected to a port, as described below.Using (4.3), we first converted the amplitude and phase of the 5150 µm transmision line's S_{11}, S_{12}, S_{21}

and S_{22} parameters from degrees and decibles to real and imaginary numbers as it will be required later,

$$S_{ij} = (10\text{^}(S_{ij5150}./20))*(i.*\sin(S_{ij5150p}.*pi/180)+\cos(S_{ij5150p}.*pi/180)) \quad (4.3)$$

where S_{ij5150} is the measured amplitude of the scattering parameter of the 5150 µm transmision line in dB, and $S_{ij5150p}$ is the measured phase of its scattering parameter in degree.

If we consider the 5150 µm CBCPW structure including its two port as a cascade of two 2575 µm CBCPW lines, each with one port, we can write the following relation for the overall transmission parameters (T parameters) of the 5150 µm line as

$$T_{A1}.T_{A2}=T_{5150} \qquad (4.4)$$

where T_{A1} and T_{A2} are the T parameters of each half of the 5150 µm line including the input and output ports. If we calculate T_{A1} and T_{A2} we can obtain the scattering parameters of a 2575 µm line including the dummy ports by converting its T parameters to S parameters. In order to do so, we first write the T parameters of the two test fixtures as a function of their S parameters in Equation 4.4 resulting in the following four equations to be solved simultaneously,

$$(S_{12A1}*S_{21A1} - S_{11A1}*S_{22A1})*(S_{12A2}*S_{21A2} - S_{11A2}*S_{22A2})/(S_{21A1}*S_{12A2}) - S_{11A1}*S_{11A2}/(S_{21A1}*S_{12A2}) = (S_{125}*S_{215} - S_{115}*S_{225})/S_{125}$$

$$(S_{12A1}*S_{21A1} - S_{11A1}*S_{22A1})*S_{22A2}/(S_{21A1}*S_{12A2}) + S_{11A1}/(S_{21A1}*S_{12A2}) = S_{115}/S_{215}$$

$$S_{22A1} * (S_{12A2} * S_{21A2} - S_{11A2} * S_{22A2}) / (S_{21A1} * S_{12A2}) + S_{11A}1 / (S_{21A2} * S_{12A2}) = S_{225} / S_{215}$$

$$- S_{22A1}\text{^}2 / (S_{21A1} * S_{12A2}) + 1 / (S_{21A1} * S_{12A2}) = 1 / S_{215}. \quad (4.5)$$

Since the two test fixtures are exactly the same except that the input and output are swapped, we can conclude that their S parameters are identical if we change their input port and output port in the matrix,

$$S_{11A1} = S_{22A2}$$

$$S_{22A1} = S_{11A2}$$

$$S_{12A1} = S_{21A2}$$

$$S_{21A1} = S_{12A2}. \qquad (4.6)$$

Using the above equalities, we can simplify the four equations to

$$(S_{12A} * S_{21A} - S_{11A} * S_{22A})\text{^}2 / (S_{21A} * S_{12A}) - S_{11A}\text{^}2 / (S_{21A} * S_{12A}) = (S_{125} * S_{215} - S_{115} * S_{225}) / S_{125}$$

$$(S_{12A} * S_{21A} - S_{11A} * S_{22A}) * S_{22A} / (S_{21A} * S_{12A}) + S_{11A} / (S_{21A} * S_{12A}) = S_{115} / S_{215}$$

$$S_{22A} * (S_{12A} * S_{21A} - S_{11A} * S_{22A}) / (S_{21A} * S_{12A}) + S_{11A} / (S_{21A} * S_{12A}) = S_{225} / S_{215}$$

$$- S_{22A}\text{^}2 / (S_{21A} * S_{12A}) + 1 / (S_{21A} * S_{12A}) = 1 / S_{215}. \quad (4.7)$$

In order to further simplify the above equations, we need to review the properties of the reciprocal networks. In a reciprocal network, the power losses are equal between any two ports regardless of the direction of propagation, that is $S_{21}=S_{12}$ for a two-port network. If a network is passive and contains only isotropic materials, we can categorize it as a reciprocal network. For instance, cables, attenuators, and all passive power splitters and couplers are reciprocal networks [51].

On the other hand we have non-reciprocal networks in which the scattering parameter S_{21} is much different from S_{12}. Obviously non-reciprocal networks contain anisotropic materials such as the class of materials known as ferrites, from which circulators and isolators are made. In anisotropic materials, depending on which direction a signal propagates, the electrical properties such as the relative dielectric constant would be different [51]. We categorized the RF amplifiers and isolators as non-reciprocal networks, because the scattering parameter S_{21} is very different from S_{12}.

Since our network is passive and contains only isotropic materials, we have a reciprocal network, which means $S_{21A}=S_{12A}$ and $S_{215}=S_{125}$.

Thus we can simplify the previous sets of equations in (4.7) to the equations in (4.8). Matematica software is utilized to solve the above equations which ultimately results in the scattering parameters of a 2575 μm line including the dummy ports,

$$(S_{12A}\text{^}2 - S_{11A} * S_{22A})\text{^}2 / S_{12A}\text{^}2 - S_{11A}\text{^}2 / S_{12A}\text{^}2 = (S_{125}\text{^}2 - S_{115}\text{^}2) / S_{125}$$

$$(S_{12A}\text{^}2 - c^* S_{22A})^* S_{22A} / S_{12A}\text{^}2 + S_{11A} / S_{12A}\text{^}2 = S_{115} / S_{125}$$

$$- S_{22A}\text{^}2 / S_{12A}\text{^}2 + 1 / S_{12A}\text{^}2 = 1 / S_{125} . \quad (4.8)$$

Having calculated the T parameters of the test fixtures, the final step would be to calculate the T parameters of the DUT of the 5000 µm CBCPW line using

$$T_{A1}.T_{5000}.T_{A2}=T_{10150} , \quad (4.9)$$

where, T_{A1} *and* T_{A2} are the T parameter matrix of the 2575 µm transmission lines and their dummy ports which were calculated previously. Converting the measured S-parameters of the 10150 um CBCPW line to the T-parameters, we can compute the T-parameters of the 5000 um CBCPW line using

$$T_{5000} = T_{A1}^{-1} \cdot T_{10150} \cdot T_{A2}^{-1} . \quad (4.10)$$

Equation 4.10 produces the scattering parameters of the de-embedded 5000 µm CBCPW based on the proposed de-embedding method.

4.5 Dielectric Characterization Results

Using the Conformal Mapping Technique described in Chapter 3 enables us to calculate the dielectric properties of the LTCC based on the new de-embedding method. The results are more accurate, since the electromagnetic field of the de-embedded line with the proposed technique is much more similar to the original line than the conventionally de-embedded lines. Figure 4.6 shows the loss tangent of the Dupont 951 LTCC utilizing the measurement results after de-embedding up to 10 GHz using our proposed technique.

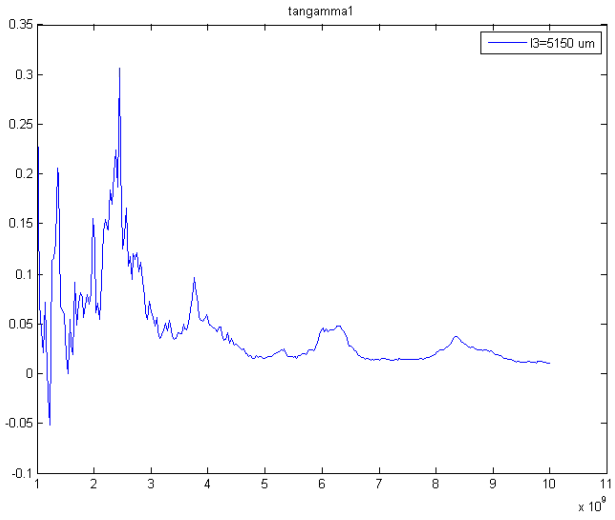

Figure 4.6. Loss tangent of Dupont 951 LTCC using measurement results after de-embedding up to 10 GHz using our proposed analytical method.

Table 4.1 represents the improved loss tangent of the LTCC which verifies the superior performance of our proposed de-embedding analytical technique.

Table 4.1. Improved loss tangent of Dupont 951 LTCC.

Frequency GHz	Loss Tangent
0.5	0.01
1	0.01
2	0.01
3	0.01
4	0.007
5	0.009
6	0.006
7	0.01
8	0.008
9	0.009
10	0.01

4.6 Modeling of Other LTCC Devices

For modeling LTCC devices such as transmission lines, capacitors, inductors and other passive elements, one can easily take advantage of the available Agilent models and simply replace the loss tangent and dielectric constant of the Dupont 951 LTCC reported in Table 4.1.

Figure 4.7 shows a sample stripline and its substrate characteristics. In Figure 4.8 we demonstrated that the substrate properties can be defined according to the loss tangent and dielectric constant reported in Table 3.4 and Table 4.1 at the desired frequencies.

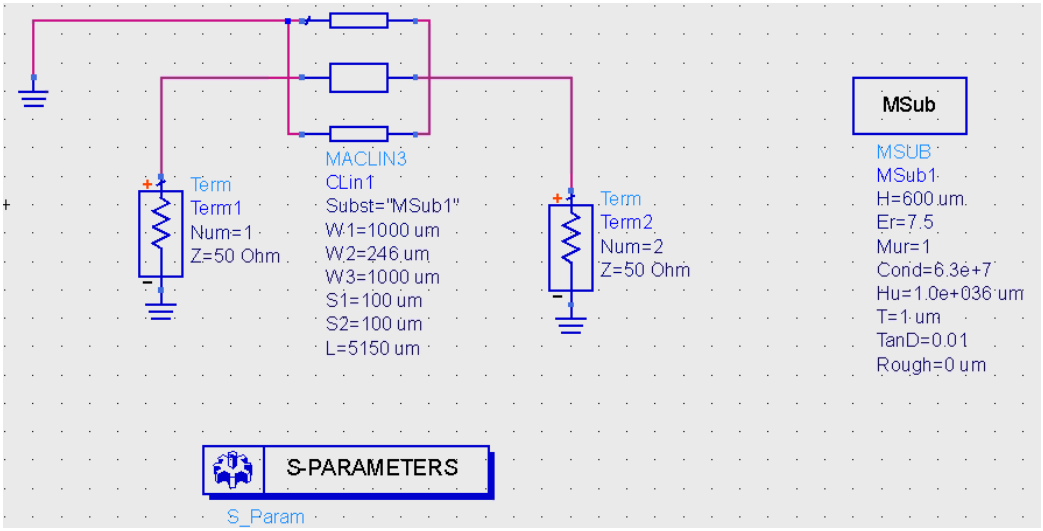

Figure 4.7. Model of stripline in ADS assuming Dupont 951 LTCC as its substrate.

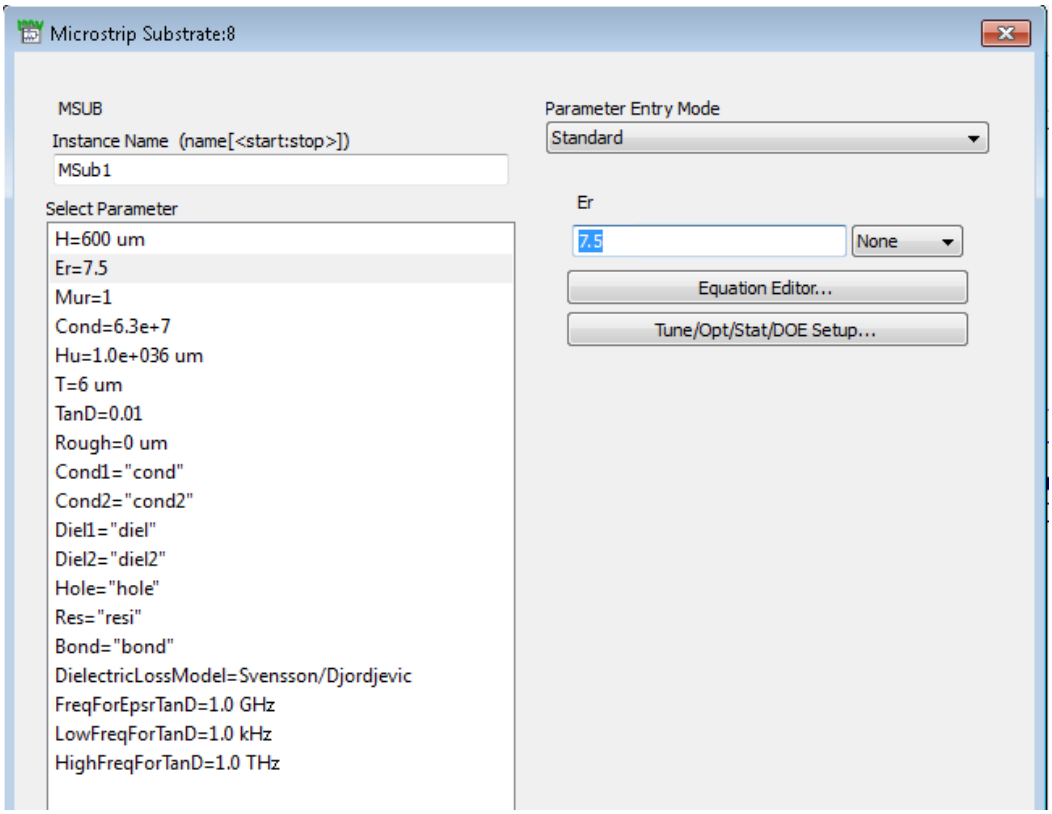

Figure 4.8. Creation of the substrate of Dupont 951 LTCC for a stripline in ADS.

However, there have been considerations in the LTCC design kits in contrary to the design kits developed for MMIC's and RFIC's [50].

There are no industry standards for a LTCC design kit, but there are many other variables such as dielectric, metallization, resistance layers, and geometry, via size and placement of the cavities. As mentioned earlier there are different numbers of layers in the LTCC, as well as in embedded RF components and integrated active devices which may be on any layer.

The Ansoft designer has some features for LTCC such as fully parameterizable geometry and arbitrary two dimensional and three dimensional vias. There are

variable stack-up properties such as the thickness or height of the material or conductor, and the dielectric constant of the material and the conductivity of the metal [51].

4.7 Summary

In Chapter 4 we presented a novel de-embedding technique that removes the effects of test fixtures such as ports more accurately compared to the convention de-embedding methods.

In fact, the proposed method not only de-embedded the pad, but also certain lengths of the transmission line connecting the pads to the device under test leaving the electromagnetic field around de-embedded structure relatively unchanged from that of the original structure. This produced more accurate measurement results for the de-embedded structure. Based on the proposed method, we characterized the LTCC dielectric material with more accurate results for the loss tangent of the material compared to the previously calculated parameters based on the conventional method, and consequently more accurate characterization of the LTCC material.

Chapter 5

Conclusions

The focus of this dissertation was on the characterization of Low Temperature Co-fired Ceramic (LTCC) for microwave and Radio Frequency (RF) applications. In this work, the LTCC dielectric parameters were characterized from 100 MHz to 10 GHz. To estimate the dielectric constant and loss tangent of a LTCC substrate, several test structures were fabricated on LTCC substrates and their S-parameters were measured using a VNA. We investigated various measurement techniques which led us to choose a parallel plate capacitor for the characterization of a LTCC substrate from 100 MHz to 1 GHz and a Conductor Backed Co Planar Waveguide (CBCPW) from 1 GHz to 10 GHz.

In Chapter 3 we designed five parallel plate capacitors and fourteen CBCPWs using Agilent App CAD and ADS EM simulations to characterize the Dupont 951 LTCC substrate from 100 MHZ to 10 GHz. To obtain the scattering parameters of the CBCPW test structures, the effects of the pads were de-embedded from the measured scattering parameters using a conventional de-embedding method. In order to de-embed the test fixture we needed to model the ports of our test structure designs as two port RLC circuits using MATLAB software. Finally, the

dielectric constant and loss tangent were calculated accurately, utilizing the Conformal Mapping Technique.

In Chapter 4 we presented a novel de-embedding technique to de-embed the 5150 μm CBCPW test structure taking advantage of the measurement results of the 10150 μm transmission line. Having the knowledge that we have a reciprocal network, some simplifications were applied to the equations and applying Matematica software solved the equations and saved us a lot of time.

We also computed the specified lines' electromagnetic field distribution using ADS FEM simulations which confirmed the similarity of the transmission lines' electromagnetic fields when they are de-embedded using our analytical technique.

The proposed method not only de-embedded the pad, but also certain lengths of transmission line connecting the pads to the device under test leaving the electromagnetic field around de-embedded structure relatively unchanged from that of original structure. This produced more accurate measurement results for the de-embedded structure, and consequently a more accurate characterization of LTCC material.

Bibliography

[1] Daniel I. Amey and Samuel J. Horowitz, “High frequency electrical characterization of electronic packaging materials: environmental and process considerations”, *International Symposium on Advanced Packaging Materials,* 1998.
[2] Antonije R. Djordjevic and Radivoje M. Biljic, “Wideband frequency-domain characterization of FR-4 and time-domain Causality”, *IEEE Transactions on Electromagnetic Compatibility,* Vol. 43, No.4, November 2001.
[3] Research Triangle Park, “Characterization of low loss LTCC material at 40 GHz” DuPont Microcircuit Materials, NC, *Microwave Journal*, 2001.
[4] Daniel I. Amey and Joseph P. Curilla, “Microwave properties of ceramic materials”, *IEEE Microwave Journal,* 1991.
[5] Ke-Li Wu and Lap Kun Yeung, “An efficient PEEC algorithm for modeling of LTCC RF Circuits with finite metal strip thickness”, *IEEE Microwave and Wireless Components Letters*, Vol. 13, No. 9, September 2003.
[6] Charles Free and Zhengrong Tian, “A new LTCC fabrication technology for planar millimeter-wave circuits”, *IEEE Microwave Conference*, Vol. 3, 1999.
[7] P.C. Donohue, et al., "A new low loss lead free LTCC system for wireless and RF applications," *Proceedings of the International Conference on Multichip Modules and High Density Packaging*, pp. 196-199, 1998.
[8] Altsculer H.M., M. Sucher and J. Fox ed., “Dielectric constant”, *Chapter IX of Handbook of Microwave Measurements*, Wiley, 1963.
[9] J. Baker-Jarvis, M. D. Janezic, J. S. Grosvenor, R. G. Geyer, “Transmission/reflection and short-circuit methods for measuring permittivity and permeability”, *NIST Technical Note 1355-R*, December 1993.
[10] Application Note 1369-1, “Solutions for measuring permittivity and permeability with LCR meters and impedance analyzers”, *Agilent Literature Number 5980-2862EN*, May 6, 2003.
[11] Toshio Nishikawa and Youhei Ishikawa, “Precise measurement method for complex permittivity of microwave dielectric substrate”, *CPEM ’88 Digest*, Japan, 2001.
[12] Application note 1287-1,” Understanding the fundamental principles of vector network analysis”, *Agilent literature number 5965-7707E*, 2000.
[13] Application note 1287-2, “Exploring the architectures of network analyzers”, *Agilent literature number 5965-7708E*, December 6, August 2000.
[14] J. Krupka and R. G. Geyer, “Measurements of the complex permittivity of microwave circuit board substrates using split dielectric resonator and reentrant cavity techniques”, *International Conference on Dielectric Materials Measurements and Applications*, No. 43, September 1996.
[15] Application note 1287-3, “Applying error correction to network analyzer measurements”, *Agilent literature number 5965-7709E*, March 27, 2002.
[16] Ann-Laure Franc and Emmanuel, “Characterization of thin dielectric films up to Mm-wave frequencies using patterned shielded coplanar waveguides”, *IEEE Microwave and Wireless Components Letters*, Vol. 22, No. 2, February 2012.
[17] D. V. Blackham, R. D. Pollard, “An improved technique for permittivity measurements using a coaxial probe”, *IEEE Transactions on Instrumentation and Measurement,* Vol. 46, No 5, pp. 1093- 1099, October 1997.
[18] Technical Overview, “Agilent 85071E materials measurement software”, *Agilent literature number 5989-0222EN*, November 6, 2003.
[19] Technical Overview,” Agilent 85070E dielectric probe kit 200 MHz to 50 GHz”, *Agilent literature number 5988-9472EN*, May 9, 2003.
[20] “ASTM Test methods for complex permittivity (Dielectric Constant) of solid electrical insulating materials at microwave frequencies and temperatures to 1650°”, *American Society for Testing and Materials*, ASTM Standard D2520.
[21] Application Note 380-1, “Dielectric constant measurement of solid materials using the 16451B dielectric test fixture”, *Agilent literature number 5950-2390*, September 1998.

[22] Albert Sutono and Deukhyoun Heo, "High-Q LTCC-based passive library for wireless system-on-package (SOP) module development", *IEEE Transactions on Microwave Theory and Techniques*, Vol. 49, No. 10, October 2001.
[23] H. E. Bussey, "Measurement of RF properties of materials-A survey", *Proceedings of the IEEE*, Vol.56, No.4, pp.729, April 1968.
[24] A. C. Lynch, "Precise measurements on dielectric and magnetic materials", *IEEE Transactions on Instrumentation and Measurement*, Vol. IM-23, No. 4, pp. 425, December 1974.
[25] M. Afsar, J.B. Birch, R.N. Clarke, Ed. G.W. Chantry, "Measurement of the Properties of Materials", *Proceedings of the IEEE*, Vol. 74, No. 1, pp. 183-199, January 1986.
[26] A. M. Nicolson, G. F. Ross, "Measurement of the intrinsic properties of materials by time-domain techniques", *IEEE Transactions on Instrumentation and Measurement*, Vol. 19, pp. 377-382, November 1970.
[27] W. B. Weir," Automatic measurement of complex dielectric constant and permeability at microwave frequencies", *Proceedings of the IEEE*, Vol. 62, No. 1, pp. 33-36, January 1974.
[28] M. T. Sebastian and H. Jantunen, "Low loss dielectric materials for LTCC applications: a review ", *International Materials Reviews*, Vol. 53, No. 2008.
[29] Liang Chai, Aziz Shaikh, Vern Stygar," Characterization of LTCC material systems at microwave frequencies", *IMAPS Advanced Technology Workshop on Ceramic Technologies for Microwave*, March 26-27, 2001.
[30] Janina Mazierskaa, Mohan V. Jacoba, Andrew Harringa, Jerzy Krupkab, Peter Barnwellc, Theresa Simsc," Measurements of loss tangent and relative permittivity of LTCC ceramics at varying temperatures and frequencies", *Journal of the European Ceramic Society*, 2003.
[31] J. Zhang CISCO Systems, Inc. CA, USA M. Y. Koledintseva," Planar transmission line method for characterization of printed circuit board dielectrics", *Progress In Electromagnetics Research*, PIER 102, 2010.
[32] Giovanni Ghione and Michele Goano, "The influence of ground-plane width on the ohmic losses of coplanar waveguides with finite lateral ground planes", *IEEE Transaction on Microwave Theory and Technique*, Vol. 45, No. 9, September 1997.
[33] Deepkumar Nair, K.E. Souders, K.M. Nair, M.F. McCombs, J.M. Parisi, Brad Thrasher," DuPont Microcircuit Materials, DuPont™ GreenTape™ 9K7 low temperature co-fired ceramic material system for RF/Microwave Packaging Applications", *The Miracles of Science*,2002.
[34] "Agilent basics of measuring the dielectric properties of materials application note agilent technologies, Inc." *Printed in USA*, June 26, 2006.
[35] Roger. B. Marks, "A multiline method of network analyzer calibration", *IEEE Transactions on Microwave Theory and Techniques*, Vol. 39, No. 7, July 1991.
[36] Cletus A. Hoer, "Choosing line lengths for calibrating network analyzers", *IEEE Transactions on Microwave Theory and Techniques*, Vol. 31, No.1, pp.76,78, January 1983..
[37] Felix D. Mbairi and Hjalmar Hesselbom, "High frequency design and characterization of SU-8 based conductor backed coplanar waveguide transmission lines", *International Symposium on Advanced Packaging Materials: Processes, Properties and Interfaces*, pp. 243-248, 16-18 March 2005.
[38] Julien Fleury and Olivier Bernard, "Designing and characterizing TRL fixture calibration standards for device modeling", *Applied Microwave and Wireless*, 2005.
[39] "Determining dielectric constants using a agilent de-embedding and embedding S-parameter networks using a vector network analyzer" *Application Note 1364-1 Agilent Technologies*, , May 30, 2004.
[40] T. T. Grove, M. F. Masters, and R. E. Miers, "Parallel plate capacitor", *American Association of Physics Teachers*, 2005.
[41] M. Henry', C. E. Free', Q. Reynolds2, S. Malkmus2, and J. ood,"Electrical characterization of LTCC coplanar lines up to 110 GHz", *Proceedings of the 36th European Microwave Conference*, Manchester UK, September 2006.
[42] Hirai, "Design guidelines for LTCC", 2009.
[43] Brian C. Wadell,"Transmission line design handbook", 1991.
[44] Lawrence M. Burns,"RF & microwave design techniques for PCBs", *Proceedings PCB Design Conference West*, 2000.

[45] Andy Kowalewski, PhillipsCorporation," Partitioning for RF design", *Printed Circuit Design Magazine*, April 2000.
[46] Gupta, Garg, Bahl and Bhartia, "Microstrip lines and slotlines", 1996.
[47] Rick Hartley,"RF / Microwave PC board design and layout base materials for high speed high frequency PC boards*", http://www.qsl.net/va3iul/.*
[48] "A guide to better vector network analyzer calibrations for probe-tip measurements", *Cascade Microtech Inc*., Copy right 1994.
[49] Tim Mobley and Glen Oliver," Filter design flow and implementation in LTCC," *partners in Design, Ansoft,* 2006.
[50] Karl-Heinz Drue and Heiko Thust, "RF models of passive LTCC components in the lower gigahertz-range", *Applied Microwave and Wireless,* April 1998.
[51] Liam Devlin, Graham Pearson, Jonathan Pittock, "RF and microwave component development in LTCC," *C-MAC MicroTechnology,* February 2001.